BIOPHYSICAL CHARACTERIZATION OF THE GM2 ACTIVATOR PROTEIN BY SITE DIRECTED SPIN LABELING ELECTRON PARAMAGNETIC RESONANCE SPECTROSCOPY

By

JORDAN DELYN MATHIAS

A DISSERTATION PRESENTED TO THE GRADUATE SCHOOL
OF THE UNIVERSITY OF FLORIDA IN PARTIAL FULFILLMENT
OF THE REQUIREMENTS FOR THE DEGREE OF
DOCTOR OF PHILOSOPHY

UNIVERSITY OF FLORIDA

2009

To my grandparents Fred and Mary Slade and to my parents Barry and Wendy Mathias

ACKNOWLEDGMENTS

I am very grateful for my parents Barry and Wendy Mathias and my sister Zoe Mathias who gave me endless love and support during graduate school. I would like to thank my grandparents Fred and Mary Slade who encouraged me to go to graduate school to begin with. It is because of their influence and their value of education that I have accomplished this degree.

I would like to give my sincerest thanks to my graduate research advisor and mentor, Dr. Gail E. Fanucci. Her guidance has made my graduate school experience richer than I ever imagined. She has taught me a wealth of science and has inspired me, by example, to strive to exceed my own perceived abilities. She has allowed me to attend many regional and national scientific conferences that have certainly contributed to my growth as a scientist.

I would like to thank our collaborators on this project, specifically Christine Schubert Wright for the crystallography work and for teaching me the purification protocol, and Jeremiah Tipton and Alan Marshall for the mass spectrometry work in verifying proper disulfide connectivity and spin label location for the cysteine mutants.

I wish to thank the members of the Fanucci Group, especially Luis Galiano for numerous stimulating scientific discussions, for teaching me more physical chemistry than I ever wanted to know and for his genuine friendship. I also thank Yong Ran, Mandy Blackburn, Jamie Kear, Natasha Hurst, and Jeffrey Carter for their help and ideas on my project and for their friendship.

I would also like to thank three of my most influential science professors, Dr. Kelli Slunt, Dr. Leanna Giancarlo, and Dr. Susan Matts. They are my inspiration for becoming a college chemistry professor.

Finally, I would like to acknowledge several important friends who have been special people in my life throughout graduate school: Dr. Brent and Valerie Feske, Dr. Neil Stowe, Dr. Jennifer McMillan Noto and Juliana D'Andrilli.

TABLE OF CONTENTS

page

LIST OF TABLES

LIST OF FIGURES

LIST OF ABBREVIATIONS

BMP	Bis(monoacylglycero)phosphate
CD	Circular dichroism
CF	Center field
CrOx	Chromium (III) oxalate
cw-EPR	Continuous wave electron paramagnetic resonance
CYS	Cysteine
DDHPE	*N*-(5-dimethylaminonaphthalene-1- sulfonyl)-1,2-dihexadecanoyl-sn-glycero-3-phosphoethanolamine, triethylammonium salt
DNA	Deoxyribonucleic acid
DOGS-NTA-Ni	1,2-Dioleoyl-sn-glycero-3-[(*N*-(5-amino-1-carboxypentyl)iminodiacetic acid)succinyl] (nickel salt, in chloroform)
EDTA	Ethylenediaminetetraacetic acid
EPR	Electron paramagnetic resonance
GalNAc	N-acetylgalactosamine
GHz	Gigahertz
GM2AP	GM2 Activator Protein
Hex A	beta-Hexosaminidase A
HF	High field
HSQC	Heteronuclear single quantum coherence
IPTG	Isopropyl-β-D-thiogalactoside
kDa	Kilodalton
LF	Low field
LUV	Large unilamellar vesicle
M6P	Mannose-6-phosphate receptor
MOMD	Microscopic order macroscopic disorder

MTSL	Methanethiosulfonate spin label
MUGS	4-methylumbelliferyl 2-acetamido-2-deoxy-beta-D-glucopyranoside-6-sulfate
NaOAc	Sodium acetate
NeuNAc	N-acetylneruaminic acid
NH_4Ac	Ammonium acetate
Niacac	Nickel (II) acetylacetonate hydrate
NiEDDA	Nickel ethylenediamine diacetic acid
NMR	Nuclear magnetic resonance
OD	Optical density
PDB	Protein data bank
POPC	1-Palmitoyl-2-oleoyl-sn-glycero-3-phosphocholine
R-18	Octadecylrhodamine
RNA	Ribonucleic acid
SAPs	Sphingolipid activator proteins
SAPLIPs	Saposin like proteins
SDSL	Site directed spin labeling
SP-B	Surfactant protein B
TIM	Triose isomerase
WT	Wild type

Abstract of Dissertation Presented to the Graduate School
of the University of Florida in Partial Fulfillment of the
Requirements for the Degree of Doctor of Philosophy

BIOPHYSICAL CHARACTERIZATION OF THE GM2 ACTIVATOR PROTEIN BY SITE DIRECTED SPIN LABELING ELECTRON PARAMAGNETIC RESONANCE SPECTROSCOPY

By

Jordan Delyn Mathias

May 2009

Chair: Gail E. Fanucci
Major: Chemistry

Gangliosides are found in high concentrations in the plasma membranes of neuronal cells. Their catabolism, a vital process for normal cell function, is carried out by sequential cleavage of sugar groups by exohydrolases that require accessory proteins for activity. The GM2 Activator Protein (GM2AP) specifically recognizes ganglioside GM2 and presents the oligosaccharide group to beta-hexosaminidase A (Hex A) for cleavage. Mutations in Hex A and GM2AP lead to a build up of GM2, causing neurodegenerative diseases such as Tay Sachs disease or AB variant gangliosidosis.

This work utilized site directed spin labeling (SDSL) and electron paramagnetic spectroscopy (EPR) to determine the membrane bound orientation of GM2AP on lipid bilayers and to investigate conformational changes of mobile loops. A paramagnetic nitroxide radical, (1-oxyl-2,2,5,5,-tetramethyl-Δ^3-pyrroline-3-methyl) methanethiosulfonate (MTSL), was attached to GM2AP via disulfide bond to a non-native cysteine residue. Continuous wave power saturation experiments were used for measuring changes in the EPR relaxation properties of spin labeled proteins in the presence of a surface bound paramagnetic collider, DOGS-NTA-Ni, to determine a membrane bound orientation of GM2AP on phosphatidylcholine bilayers. Collision values with

DOGS-NTA-Ni were used to map regions of the protein that were accessible and inaccessible to the surface bound collider. Sites of high collision (T90R1, L126R1, and N136R1) were interpreted to be located near the bilayer surface, which corresponded to an orientation where the face of the lipid binding cavity lies on the bilayer surface.

Conformational changes of two flexible loops (spanning residues 58-62 and 122-136) were also investigated using SDSL EPR. Continuous wave EPR spectra for six spin labeled sites in these two loops in the presence and absence of GM2 micelles did not reflect changes in mobility associated with a conformational change upon ligand binding. Including the six loop sites, solution EPR spectra of four additional spin labeled sites were obtained and fit using the microscopic order macroscopic disorder (MOMD) model. The six spectra from the flexible loop sites required two components to obtain a best fit. Temperature studies suggested that the 122-136 loop was in conformational exchange, but the 58-62 loop showed no temperature dependent correlation to protein dynamics.

CHAPTER 1
INTRODUCTION TO THE GM2 ACTIVATOR PROTEIN

Gangliosides

Gangliosides are a type of glycosphingolipid that are essential components of eukaryotic cell membranes. They form specific patterns on the cell surface that function as markers that change upon cell differentiation (*1, 2*). Functions of gangliosides include serving as binding sites for bacteria, viruses and toxins (*3*), interacting with membrane bound receptors and enzymes (*4, 5*), and participating in cell-cell interactions (*6*). In many cases, the sialic acid residue, a sugar unique to gangliosides, is the group that is recognized by bacterial or viral binding proteins or by membrane receptors (*7*). Metabolic products of ganglioside degradation, including sphingosine and ceramide, have roles in signal transduction. Finally, gangliosides and other glycosphingolipids can function as a protective layer on biological membranes to prevent inappropriate degradation.

Glycosphingolipids are comprised of a hydrophilic oligosaccharide chain and a hydrophobic sphingosine backbone, through which one fatty acid tail is bound through an amide bond (Fig 1-1). Variations in glycosphingolipids arise from the number and type of sugars in the oligosaccharide chain, as well as the type of glycosidic bonds that joins the sugar units. Many glycosphingolipids contain a unique nine carbon sugar called sialic acid (Fig 1-1), which then further classifies them as gangliosides. Sialic acid can have diversity in the substituent groups and in the specific glycosidic linkages with other sugars, and are usually located at the terminal end of the oligosaccharide chain (*7*). The two most common sialic acids are *N*-acetylneuraminic acid (Neu5Ac, or NeuNAc) and *N*-glycolylneuraminic acid (Neu5Gc, or NeuNGc), which contain an *N*-linked acetyl and a glycolyl group at carbon 5, respectively. Gangliosides are named starting with the letter G (for ganglioside) followed by the letters M, D, T or Q, which

stand for mono-, di-, tri- and quarto- indicating the number of neuraminic acid residues in the molecule, and finally a number that describes the number of core monosaccharides. The number is equal to "5-*n*", where *n* is the number of core monosaccharides. For example, the ganglioside GM1 contains one neuraminic acid residue to four core monosaccharides, whereas GD3 contains two neuraminic acid residues bound to two core monosaccharides. Some complex gangliosides also have an "a" or "b" at the end of their names, indicating that the galactose (Gal) residue nearest the ceramide backbone contains one, e.g. GD1a, or two, e.g. GT1b, neuraminic acid residues, respectively (*8*). At least twelve different gangliosides have been identified in the adult human brain (*1*).

The catabolism of gangliosides is a vital cellular process and occurs in the acidic lysosomal compartments of cells. The process begins with endocytosis of the outer membrane, where the fragments containing gangliosides are trafficked in the form of vesicles through the endosomes that serve as a lipid sorting site, where lipids are segregated and sent to the lysosomes, Golgi apparatus, or even back to the plasma membrane (*2*). Once in the lysosomes, degradation of the gangliosides occurs through sequential cleavage of terminal sugar groups by exohydrolases. Membrane bound gangliosides with carbohydrate chains containing four or fewer sugars are less accessible from the water-soluble hydrolases, and their catabolism requires an accessory protein to bind and, in most cases, extract the lipid from the vesicles. These accessory proteins are called sphingolipid activator proteins (SAPs) and are essential for the activity of the exohydrolases. Genetic mutations to the exohydrolases or to the SAPs can stop the progress of the ganglioside degradation pathway at various steps, which can result in a build-up of gangliosides in the lysosomes and ultimately in cell death. A number of lysosomal storage diseases have been studied and these diseases are collectively called gangliosidoses.

Saposins

Saposins are a family of cysteine rich proteins that interact with membranes (*9*). They are known for being heat stable and protease resistant, with their stability arising from the multiple structural disulfide bonds. Within this family are saposins A-D and the GM2 activator protein (GM2AP). They are accessory proteins that stimulate exohydrolases for the lysosomal degradation of gangliosides. Saposins A-D are encoded within the same gene and synthesized as a precursor polypeptide called prosaposin that gets proteolytically processed into the four individual proteins (*10*). They are structurally homologous in that they all contain the "saposin fold," characterized by four or five α-helical bundles stabilized by three disulfide bridges, and they have the same cysteine pairings (*11*) (Fig 1-2). GM2AP is also in the saposin family but is not structurally homologous to the other saposins because its secondary structure is predominantly β-sheet, and it is encoded by its own separate gene. GM2AP contains four structural disulfide bridges, and the connectivity of six of these cysteines is similar to the disulfide pattern of saposins A-D (Fig 1-2).

Saposin A

Saposin A (sap A) is an 84 amino acids protein with two glycosylation sites at Asn21 and Asn42 that is required for the *in vivo* degradation of galactosylceramide by galactosylceramide-β-galactosidase (*12*). *In vitro*, sap A can stimulate the enzymatic hydrolysis of [^{3}H]galactosylceramide and [^{3}H]glucosylceramide by β-galactosylceramidase and β-glucosylceramidase, respectively (*13*). The role of sap A in the degradation of galactosylceramide *in vivo* was demonstrated in a study where a C106F substitution was introduced to sap A in mice, which eliminated one of the disulfide bonds. The mice accumulated galatosylceramide and suffered from a late-onset form of Krabbe disease (*12*, *14*). Only one

human patient with abnormal storage of galactosylceramide has been reported. In this case, the patient was found to have a three base pair deletion in the sap A gene, resulting in the deletion of a conserved valine at residue 11 (*15*).

Saposin B

Saposin B (sap B) is an 80 amino acid protein with three disulfide bonds and one *N*-linked glycosylation site at Asn21. It is responsible for stimulating the degradation of cerebroside sulfate by arylsulfatase A and of globotriaosylceramide and digalactosylceramide by α-galactosidase A, *in vivo* . Sap B has also been shown to stimulate the *in vitro* conversion of GM1 to GM2 by β-galactosidase (*16*). Its molecular weight determined from gel filtration (20 to 22 kDa) was found to be about double its mass calculated from the amino acid sequence, suggesting that sap B is a homodimer (*17*). The crystal structure, solved in 2003, also shows sap B as a dimer, where each monomer chain consists of four amphipathic α-helices that fold into a V-shape (*9*). Two monomers clasp together to form a dimer containing a hydrophobic lipid binding cavity with a volume of roughly 900 $Å^3$. Two conformations of the sap B dimer, as well as a bound phospholipid, were observed in the X-ray structure, suggesting flexibility of the dimer, which could correlate to conformational changes that take place when sap B binds lipids (*9*). A proposed mechanism is the "open" conformation of sap B can interact with lipid bilayers, promote a reorganization of the lipid alkyl chains and bind a lipid in the hydrophobic cavity. Sap B can then undergo a conformational change to a "closed" form and carry a bound lipid into solution as a protein:lipid complex. The features of the X-ray structure are consistent with the previous observation that sap B can act as a lipid transport protein in the absence of degrading enzymes (*18*). An inherited mutation to the gene encoding for the sap B protein, resulting in the mutation of a polar threonine residue to a nonpolar isoleucine residue at amino acid 23, is

thought to prevent the glycosylation at the aspragine located two residues amino terminal to this site. This mutation causes an accumulation of cerebroside sulfate and a disease called metachromatic leukodystrophy (*19*).

Saposin C

Saposin C (sap C) is an 80 amino acid protein that, like sap B, has three disulfide bonds and forms a homodimer. It has a conserved *N*-linked glycosylation site at Asn22. Sap C is required for the lysosomal degradation of glucosylceramide by glucosylceramide-β-glucosidase. Genetic mutations that affect the function of either the sap C or the enzyme cause Gaucher's disease. The solution NMR structure of the sap C monomer consists of five α-helices that fold into half of a sphere (*20*). Two of the three disulfide bonds connect helices I and IV and the third disulfide bridges the loop between helices II and III with helix III. The function of sap C has been shown to be unaffected by the presence or absence of the oligosaccharide at Asn22 (*21*). It has also been shown that the presence of both sap A and sap C together activates the glucosylceramide-β-glucosidase degradation of glucosylceramide more than the sum of the activation induced by the two proteins separately (*22*). From this finding, it has been suggested that saposins could possibly work synergistically to accomplish their function. Although the exact mechanism of activation is still now well understood, a model has been proposed in which sap C activates glucosylceramide-β-glucosidase at the membrane surface (*16, 22*).

Saposin D

Saposin D (sap D) is an 80 amino acid protein that has one *N*-linked glycosylation site at Asn20. Sap D stimulates the degradation of ceramide to fatty acid and sphingosine by acid ceramidase in cultivated fibroblasts (*23*) and *in vitro* (*24*), and has also been shown to activate sphingomyelinase (*25*). The structure of sap D more closely resembles the structures of saps A

and D by having the typical monomeric saposin fold that consists of four amphipathic helices that fold to form a hydrophobic pocket (*26*). Details of the specific physiological function of sap D remain unclear.

Saposin-Like Proteins

A number of other proteins are structurally similar to the saposins but carry out different functions and are called the saposin-like proteins (SAPLIPs). The SAPLIPs have multiple cysteines with identical disulfide bonding patterns, are of similar size, and have a similar tertiary structure as the saposins (*10*). The various activities of SAPLIPs are divided into three areas: 1) membrane targeting, 2) membrane perturbation without permeabilization, and 3) membrane permeabilization as a defense mechanism (*27*). First, proteins that are suggested to have membrane targeting activity include metallophosphoesterases (e.g. acid sphingomyelinase) and GDSL (Gly-Asp-Ser-Leu) lipases (e.g. acyloxy acylase). Acid sphingomyelinase is not only stimulated by the saposins, but it also contains a homologous saposin-like domain. Acyloxy acylase is a lipase that acts on lipopolysaccharide and a few glycosphingolipids and contains a SAPLIP domain that is covalently attached to a catalytic protein domain through a disulfide bridge (*27*). Second, the membrane perturbation group includes the saposins A-D previously discussed as well as a protein that regulates surface tension in the lung called surfactant protein B (SP-B). *In vitro*, SP-B binds and aggregates on lipid bilayers causing destabilization of the lipid organization and leads to vesicle fusion (*27-29*). Third, several of the membrane permeablilizing proteins have antimicrobial activity, such as human granulysin and porcine NK-lysin.

GM2 Activator Protein

Biosynthesis

The GM2 activator protein (GM2AP) is the fifth of the sphingolipid activator proteins (SAPs). A function of GM2AP is to bind its substrate, ganglioside GM2, and present it as a water

soluble complex so that the terminal *N*-acetylgalactosamine (GalNAc) sugar can be enzymatically hydrolyzed by the enzyme β-hexosaminidase A (Hex A). GM2AP is synthesized on ribosomes bound to the endoplasmic reticulum (ER) as a 193 amino acid preproprotein containing a 23 amino acid pre-sequence signal peptide that directs the nascent peptide into to the ER lumen and an eight amino acid pro-sequence. The pre-sequence is believed to be cleaved co-translationally, resulting in a 170 residue pro-polypeptide (*8*). The oxidizing environment of the ER lumen, the eight native cysteines form four disulfide bonds. Additionally in the ER, GM2AP is *N*-glycosylated at Asn63-Val-Thr (where numbering begins with the initiating Met as residue 1) with a preassembled oligosaccharide made of many mannose residues. However, in *Pichia pastoris*, glycosylation patterns of GM2AP were found to consist of two *N*-acetyl glucose sugars and anywhere from nine to sixteen mannose sugars (*30*). Following glycosylation, one or more mannose residues are phosphorylated in the late ER and Golgi network (*1*). This step is essential for delivery of GM2AP to the lysosomes because intracellular transport of most lysosomal proteins occurs via the mannose-6-phosphate receptor. The pro-sequence of GM2AP is removed during lysosomal processing of the N-terminus, resulting in the active 162 residue protein. Depending upon the oligosaccharide composition, the molecular weight of glycoslyated GM2AP ranges from 20 kDa to 27 kDa (*8*).

Structure of the GM2 Activator Protein

Two different numbering schemes have been adopted as a result of the preprosequence. One style numbers the final GM2 activator protein residues from 32-193, while the other style numbers these same residues 1-162. The latter method (1-162) is used in this dissertation. The X-ray structure has been solved for non-glycosylated GM2AP purified from *Escherichia coli* (Fig 1-2). GM2AP folds into a single globular domain of approximately 45Å x 28 Å x 25 Å. The

secondary structure consists of eight β-strands that fold into a β-cup topology. The interior of the β-cup makes up a lipid binding cavity, with dimensions 12 Å x 14 Å x 22 Å and a volume that is nearly six times larger than the volume of a ceramide moiety (500 $Å^3$). Most of the amino acids that line the inside of the cavity are hydrophobic residues, which is appropriate for binding lipid hydrophobic tails. Four disulfide bonds stabilize several flexible loop regions of GM2AP and are thought to be the reason for its high stability. Another interesting feature of GM2AP structure is that it contains 16 proline residues, six of which are in the *cis*-peptide conformation (*31*). GM2AP also contains a short 2.5 turn α-helix that is the putative sight of interaction with Hex A (*32*).

Residues spanning sites 58-78, 87-97, and 120-133 were identified as loop regions with structural flexibility according to structural refinement analysis of the X-ray structure. These residues exhibited high B-factors and were found in different conformations for different GM2AP monomers within a unit cell (*31*). The loop regions line the entrance to the lipid binding cavity, suggesting that their positional differences may correlate with protein function. The most flexible of these regions is the loop that spans residues 120-133, highlighted in red (Fig 1-2). This loop is particularly important because it forms one side of the cavity opening and significantly changes the diameter of the cavity entrance. In monomers A and B, the position of the loop appears to be in a "closed" conformation, where the amino acid side chains are pointed towards the inside of the hydrophobic pocket, but in an "open" conformation in monomer C with the side chains rotated outward (Fig 1-3). These two positions change the opening to the entrance of the hydrophobic cavity from 10 Å to 13 Å and likely represent important conformational states of GM2AP (*31*, *33*).

Function of the GM2 Activator Protein

In vivo, the GM2 activator protein is required for the catabolism of ganglioside GM2 that takes place in the acidic lysosomes of cells. GM2AP is a nonenzymatic accessory protein that binds and extracts GM2 from vesicles to form a protein:lipid complex and presents the oligosaccharide group for hydrolysis of the terminal *N*-acetylgalactose (GalNAc) sugar by β-hexosaminidase A (Hex A) to form GM3 (Fig 1-4). GM2AP shows the highest affinity for GM2, having K_D = 3.5 μM (*31, 34*). In the absence of GM2AP *in vitro*, Hex A is unable to hydrolyze the terminal sugar of GM2 in liposomes (*35*). A number of *in vitro* assays have been developed for studying the function of GM2AP. As a lysosomal protein, the function of GM2AP has strong pH dependence, where it binds to bilayers at acidic pH (*36*). Two of these assays measure the GM2AP-stiumlated Hex A degradation of either tritiated GM2 or the artificial substrate 4-methylumbelliferyl 2-acetamido-2-deoxy-β-D-glucopyranoside-6-sulfate (MUGS) (*35, 37*).

The function of GM2AP stimulating the hydrolysis of [^{3}H]GalNAc-GM2 by Hex A has been reported (*35, 38, 39*), and is generally described here. Hex A, purified from human placenta, and [^{3}H]GalNAc-GM2 were incubated with varying amounts of GM2AP purified from bacteria (*39*) or human kidney (*35*) at pH 4.2 for a specified amount of time. The reaction was stopped upon the addition of chloroform, buffer, and *N*-acetylgalactosamine. The liberated [^{3}H]GalNAc was separated from the unreacted GM2 by passage over an ion-exchange mini column, where the unbound fractions containing [^{3}H]GalNAc were analyzed by scintillation counting (*35, 39*). This assay was used by Werth, et al. in a very significant experiment that showed that GM2 degradation by GM2AP and Hex A is stimulated 180-fold in the presence of 25 mol% of the anionic lipid bis(monoacylglycero)phosphate (BMP) (*40*). BMP is found in elevated concentrations in the late endosomes and likely traffic gangliosides to the lysosomes. Its

role in the protein-mediated catabolism of gangliosides is not yet well understood, and it is the subject of ongoing studies in the Fanucci lab. An assay similar to the radio-labeled method has also been used where, instead of [^{3}H]GalNAc-GM2, the fluorescently labeled artificial substrate MUGS is mixed with purified Hex A and GM2AP, and the concentration of liberated methylumbelliferone is measured fluorometrically (*37*).

The function of GM2AP has also been demonstrated through a fluorescence dequenching assay that measures the ability of GM2AP to bind and transfer the fluorescent lipid octadecylrhodamine (R-18) between liposomes (*39, 41*). Briefly, GM2AP is mixed with unlabeled liposomes and a small concentration of either glycolipid or ganglioside dissolved in chloroform, so that the glycolipid or ganglioside would distribute to the liposomes or to GM2AP. Liposomes containing R-18 lipid were prepared and are self quenched due to the high concentration of R-18. The assay was initiated upon addition of R-18 liposomes to the sample. The fluorescence intensity at 590 nm increased as the R-18 lipid was transferred by GM2AP to unlabeled liposomes. This fluorescence dequenching assay was utilized to measure the ligand affinity of GM2AP and it was found that the specificity, or strength of binding, of GM2AP to various gangliosides was GM2 >> GT1b >> GM1 ≈ GM3 > GA2 (*39*). Rigat et al. also demonstrated through use of this assay that GM2AP can also bind to platelet activating factor (PAF) and, therefore, inhibit transfer of R-18. These results suggested another potential function of GM2AP as an inhibitor of PAF signaling activity (*42*).

Another lipid transfer assay has been reported where GM2AP can bind and extract a dansyl-labeled phosphatidylethanolamine lipid (DDHPE) from vesicles (*36*). Vesicles containing 20 mol% DDHPE were mixed with GM2AP and, upon extraction of DDHPE, the emission wavelength shifted from 518 nm to 484 nm, and the intensity at the 484 nm increased as GM2AP

extracted more molecules of DDHPE. This assay not only provides a means for testing the function of GM2AP but also support the hypothesis that GM2AP can also function *in vivo* as a lipid transfer protein.

Structure of β-Hexosaminidase A

Three isozymes of the exohydrolase β-hexosaminidase exist: β-hexosaminidase A (Hex A), β-hexosaminidase B (B), and β-hexosaminidase S (Hex S). All three hexosaminidases contain two subunits, where Hex A is made of one α and one β subunit, Hex B is made of two β subunits and Hex S is made of two α subunits. GM2AP stimulates the conversion of ganglioside GM2 to GM3 by Hex A and the X-ray structure of Hex A purified from human placenta has been determined (*43*). The α and β subunits interact to form an enzyme with two domains. Domain I, made of residues 23 to 168 of the α subunit and 50 to 201 in the β subunit, contains two α-helices and a six-stranded antiparallel β sheet; the function of domain I is unknown. Residues 165- to 529 of the α subunit and 202 to 556 of the β subunit make up domain II, where eight α-helices and eight β-sheets fold into a TIM barrel. The current accepted mechanism for the conversion of GM2 to GM3 is that GM2AP binds GM2 in intralysosomal vesicle, and the protein:lipid complex then forms a ternary complex with Hex A for removal of the terminal sugar. It is believed that the GM2AP:GM2 complex interacts with the α subunit of Hex A (*44*). Residues Glu323 (α subunit) and Glu335 (β subunit) of Hex A act as general bases for the protonation of the GalNAc glycosidic oxygen of GM2 (bound by GM2AP) and are located at the opening of the TIM barrel.

The GM2 Gangliosidoses

The GM2 gangliosidoses are inherited disorders that cause an accumulation of gangliosides in the lysosomal compartments of cells, particularly neuronal cells (*1*). It was

discussed earlier in this chapter that the catabolism of ganglioside GM2 requires the accessory protein GM2AP, as well as both the α and β subunits of the enzyme Hex A. Mutations that occur in the genes encoding for any three of these polypeptides can cause GM2 gangliosidosis, where the accumulation of gangliosides results in cell death. Specifically, Tay Sachs disease is caused by defects in the α subunit of Hex A, which blocks the dimerization of the two subunits to form active Hex A. In Tay Sachs disease, the β subunits still associate to form Hex B, however GM2AP does not stimulate the conversion of GM2 to GM3 by Hex B. Another version is Sandhoff's disease, first reported by Sandhoff and his colleagues in 1968 (*45*). Patients with Sandhoff's disease have a defective β subunit in both Hex A and Hex B. Finally, the third and rarest of the GM2 gangliosidoses is called Variant AB (*46*). This disorder is caused by a mutation in the gene for GM2AP that results in the point mutation Cys107Arg (forming AB variant GM2AP), and consequently removes one of the four structural disulfide bonds. In this disorder, the build up of GM2 is thought to occur because of the inability of the AB variant GM2AP:GM2 complex to bind to Hex A (*47*).

This dissertation reports biophysical experiments that contribute to understanding aspects of GM2AP function. Site directed spin labeling (SDSL) was utilized to study GM2AP using electron paramagnetic resonance (EPR) spectroscopy. Site directed mutagenesis was used to make single amino acid substitutions to cysteines at selected residues in the protein, to which a paramagnetic nitroxide spin probe was attached through formation of a covalent disulfide bond. The EPR line shapes of spin labels attached to proteins correlate to protein backbone motion, spin label motion, as well as overall tumbling of the protein in solution. Thus, SDSL EPR has been widely used for studying protein dynamics in solution (*48, 49*). The following chapters describe EPR theory, including theory of the power saturation experiment, the use of power

saturation EPR to learn how GM2AP associates with phosphatidylcholine bilayers, and the use of SDSL EPR to investigate conformational changes of flexible loop regions that are thought to interact with lipid bilayers and could possibly play a role in binding lipids.

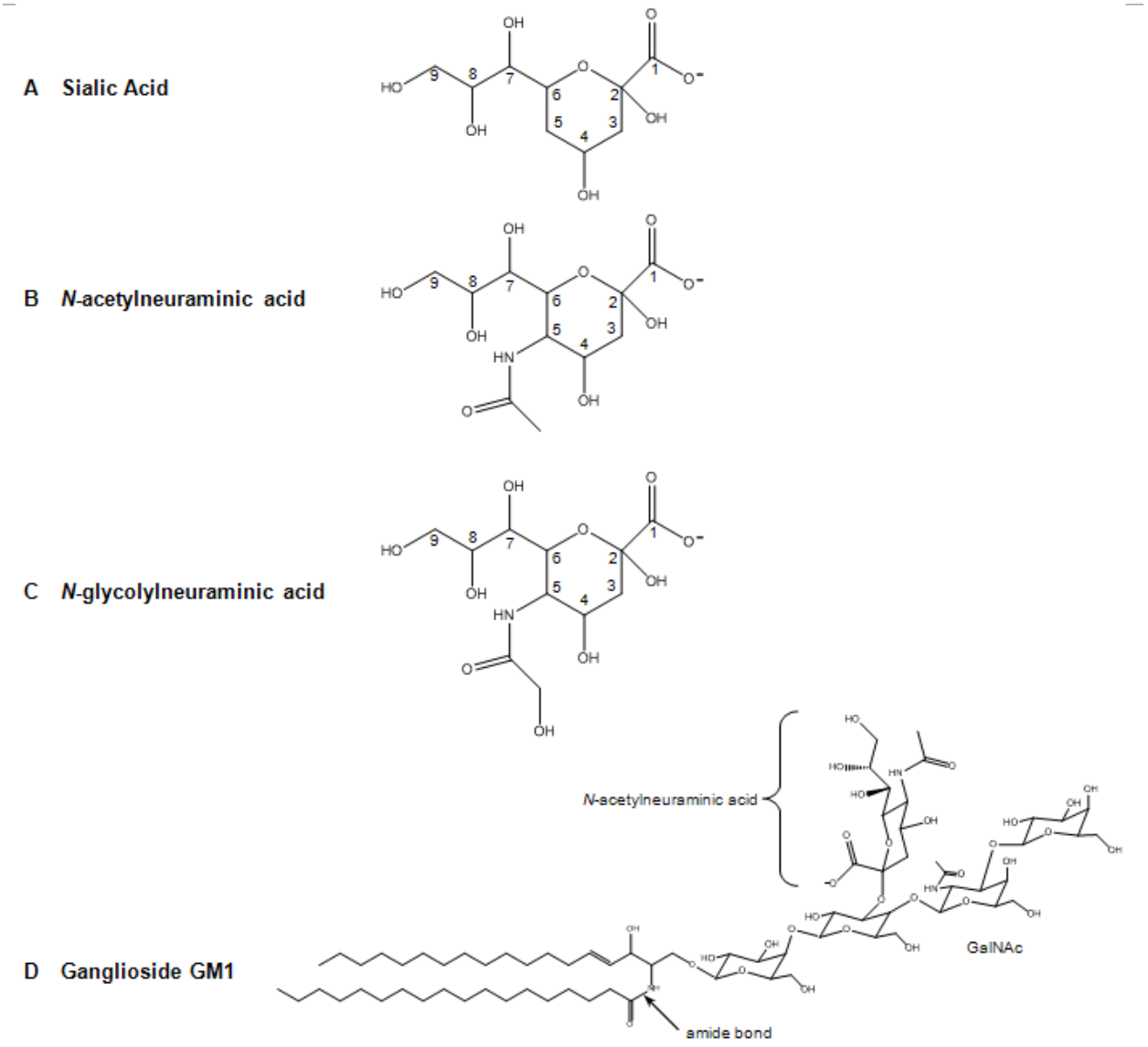

Figure 1-1. Structures of sialic acid, *N*-acetylneuraminic acid and ganglioside GM1. A) The structure of the nine carbon sugar sialic acid is shown, including the numbering of the carbon chain. Sialic acid can be derivatized at carbon 5 with an *N*-acetyl group or an *N*-glycolyl group to produce *N*-acetylneuraminic acid or *N*-glycolylneuraminic acid. B) Structure of *N*-acetylneuraminic acid, C) Structure of *N*-glycolylneuraminic acid, D) Structure of ganglioside GM1. Gangliosides are glycosphingolipids that contain a sphingosine backbone with a fatty acid attached through an amide bond and an oligosaccharide head group where at least one of the sugars is sialic acid, or one of its derivatives.

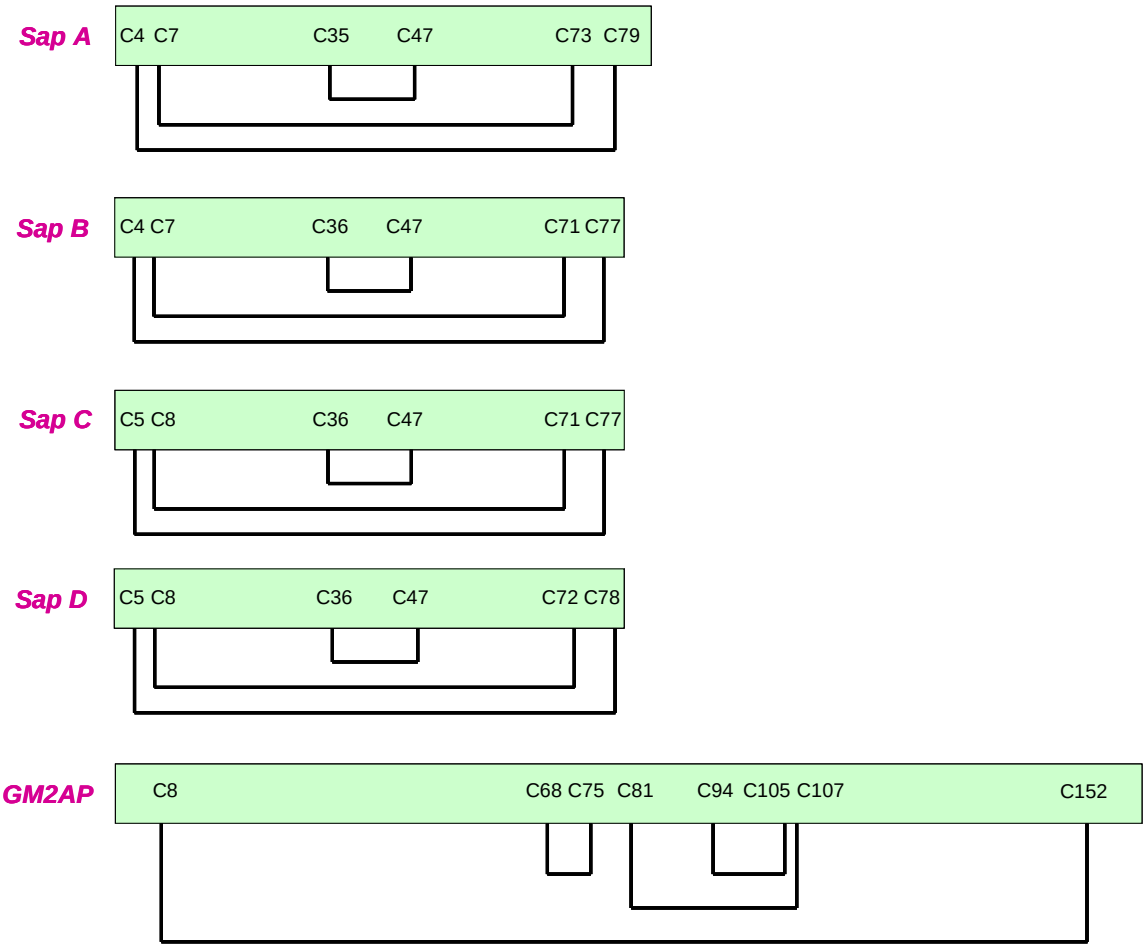

Figure 1-2. Cysteine connectivity of sphingolipid activator proteins (Saps) A-D and the GM2 Activator Protein (GM2AP). Saps A – D are synthesized as one precursor polypeptide called prosaposin, which gets proteolytically processed into the four individual proteins. Saps A-D are structurally homologous and contain multiple cysteines that have identical disulfide connectivity. GM2AP is structurally distinct from Saps A-D and has four disulfide bonds. Three of the disulfide pairings is similar to the disulfide pattern seen in Saps A-D.

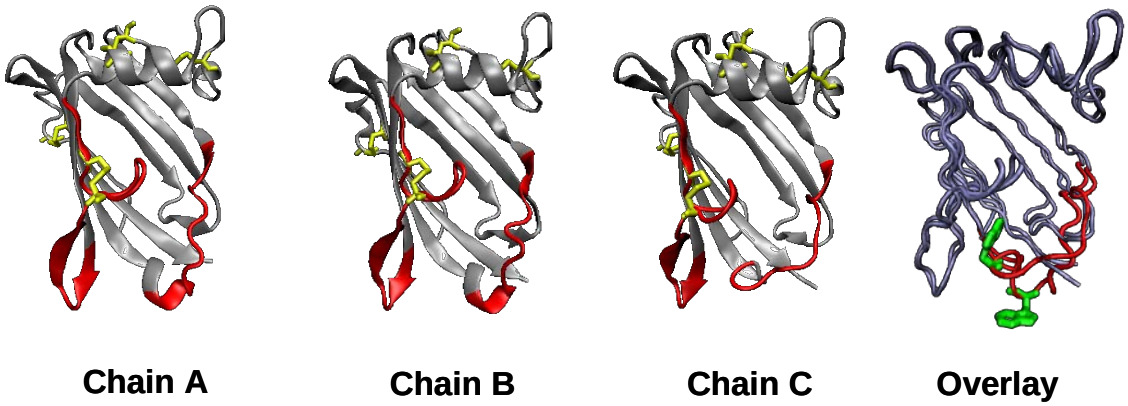

Figure 1-3. Ribbon diagram of GM2AP structures showing alternate loop conformations. The X-ray structure shows three conformations of GM2AP (PDB ID 1G13) within one unit cell. The four disulfide bonds are shown in yellow, and the regions of high flexibility are highlighted in red. The overlay of chains A and C is shown to emphasize the different conformations of this loop, with the mobile loop (residues 122 to 136) highlighted in red. In addition to positional differences in the protein backbone, the amino acid side chains are in different conformations as well, as shown by Trp63 in licorice style in green.

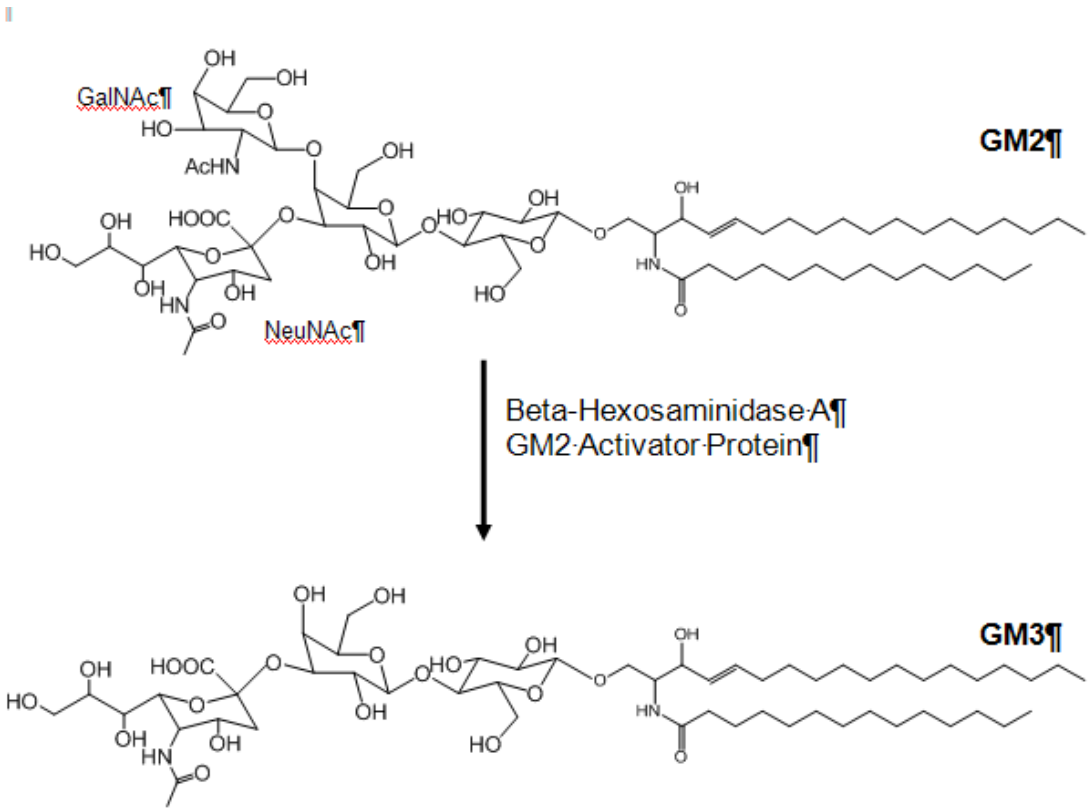

Figure 1-4. Hydrolysis reaction that converts GM2 to GM3 by the GM2 activator protein (GM2AP) and β-hexosaminidase A (Hex A). The terminal N-acteylgalactose (GalNAc) residue of GM2 is hydrolyzed by Hex A to form GM3.

Table 1-1. Protein Data Bank (PDB) identification codes and structure parameters

Protein	PDB ID	Experimental Method	Resolution (Å)	R value	R free	Space Group	Expression System
GM2AP	1g13	X-ray diffraction	2.00	0.215 (work)	0.258	$P\ 2_12_12_1$	E. coli
Sap A	2dob	X-ray diffraction	2.00	0.219 (obs.)	0.267	$P\ 2_12_12_1$	E. coli
Sap B	1n69	X-ray diffraction	2.20	0.222 (obs.)	0.262	$P\ 3_121$	E. coli
Sap C	2gtg	X-ray diffraction	2.40	0.221 (obs.)	0.283	$P\ 6_3$	E.coli
Sap C	1m12	Solution NMR					E. coli
Sap D	3bqq	X-ray diffraction	2.00	0.198 (obs.)	0.242	P 1	E. coli
Hex A	2gjx	X-ray diffraction	2.80	0.270 (obs.)	0.288	C 2 (C121)	Human placenta
Hex B	1nou	X-ray diffraction	2.40	0.203 (obs.)	0.231	$P\ 6_122$	Human placenta

CHAPTER 2
THEORY OF ELECTRON PARAMAGNETIC RESONANCE SPECTROSCOPY

Introduction to Electron Paramagnetic Resonance Spectroscopy

Electron paramagnetic resonance (EPR) spectroscopy is a magnetic resonance technique used to study paramagnetic systems, those containing unpaired electrons, with an external magnetic field. Electrons have a magnetic dipole that arises predominantly from the spin angular momentum, where electrons have spin quantum numbers $m_s = 1/2$. Systems with electrons occurring in pairs have a net magnetic moment of zero; therefore, only systems containing one or more unpaired electrons have a net magnetic moment that is suitable for interacting with an electromagnetic field (*50*). In an external magnetic field, the magnetic moment of the electron aligns itself either parallel or antiparallel to the field. This phenomenon splits the energy into two states, known as the Zeeman splitting, where the energy difference is proportional to the magnitude of the external magnetic field (B), the spectroscopic g-factor (g), and the Bohr magneton (β_e).

$$\Delta E = h\upsilon = g\beta_e B \tag{2-1}$$

The Bohr magneton is a proportionality constant defined as

$$\beta_e = \frac{e\hbar}{2m_e} \tag{2-2}$$

In this equation, e is the electric charge, $\hbar$ is the Plank constant divided by 2π (1.054×10^{-34} J·s), m_e is the mass of the electron (9.109×10^{-31} kg), and the value of the β_e is 9.274×10^{-24} J·T^{-1}. An energy level diagram for a free electron in a magnetic field is shown in Figure 2-1. Resonance occurs when the energy applied to the system (ΔE) matches the splitting in energy levels of the system. For EPR work described in this dissertation, resonance occurs at a magnetic field of about 0.33 Tesla (T) magnetic field, where the frequency is approximately 9.8 gigahertz (GHz).

This range of energy for EPR is termed X-band; other "bands" of EPR operation include the higher frequencies Q (36 GHz) and W (95 GHz) band, which require higher magnetic fields in order to meet the resonance energy requirements.

The Zeeman splitting for a free electron in a magnetic field, as just described, results in two energy levels ($m_s = \pm 1/2$). When the unpaired electron can interact with a neighboring nucleus that also has a magnetic moment, each energy level is further split because of the hyperfine interaction between the electron and nuclear spin magnetic moments. For nuclei with spin quantum number $I = 1$, the two energy levels resulting from Zeeman splitting are each split into three more energy levels for nuclear spin quantum numbers $m_I = 0, \pm 1$ (Fig. 2-2). Such a splitting pattern gives rise to three allowed transitions, since the selection rules indicate that $\Delta m_s = 1$ and $\Delta m_I = 0$.

Electron Paramagnetic Resonance of Spin Labels

Electron paramagnetic resonance spectroscopy (EPR) has become useful for studying biomolecules that do not contain an unpaired electron through the development of a technique called spin labeling. A spin label is a small molecule that contains a stable nitroxide radical and is covalently attached to biomolecules. For the case of proteins, spin labels are attached through derivatization of specific amino acid side chains. The research presented in this dissertation employed the spin label methanethiosulfonate (MTSL) that was covalently attached to cysteine side chains through the formation of a disulfide bridge (Fig. 2-3). The unpaired nitroxide radical electron couples to the nitrogen nucleus, that has spin $I = 1$, and the resulting line shape has three peaks (Fig. 2-2). The EPR spectra of spin labeled proteins have been utilized to gain insight on local dynamics of the nitroxide and/or protein backbone (*49, 51*), the orientation of proteins on

or within biological membranes (*4, 52-55*), secondary structure (*56, 57*), and the distance between two spin labels (*58, 59*).

The EPR line shape of a nitroxide spin label attached to a protein results from a convolution of motions that changes dramatically as the correlation time, τ, varies from 0.1 –50 ns at X-band EPR frequencies. The correlation time, τ, consists of three modes of motion: (1) the rotational correlation time, τ_R, or the tumbling of the entire molecule, (2) the internal correlation time, τ_i; defined by torsional oscillations about internal bonds within the nitroxide moiety and its attachment to the cysteine amino acid side chain, and (3) local dynamics, τ_B, or the local macromolecular fluctuations of the protein at the labeling site. Spin labeled proteins that are smaller than 15 – 18 kilodaltons (kDa) have fast rotational correlation times since they tumble quickly in solution and produce very isotropic, or narrow, EPR line shapes due to motional averaging. Isotropic spectra provide little information about the system, and it is usually necessary to slow the correlation time of small proteins and peptides by tethering them to larger molecules (such as a lipid vesicle or resin bead), by increasing the viscosity of the solution, or by reducing the temperature. Proteins larger than 18 kDa have slower correlation times and, therefore, have EPR line shapes that are dominated by either internal rotations (τ_i) of the spin label or by fluctuations of the protein backbone (τ_B). The major source of useful information on protein structure and dynamics in site directed spin labeling EPR studies comes from line shapes with molecular motions dominated by τ_i and τ_B.

Spectral parameters of EPR line shapes can be measured quantitatively compare EPR spectra. The most common parameters are the peak-to-peak line width (ΔH_{pp}) of the central resonance, the ratio of intensities of the low field and center field resonances (LF/CF), and the second moment ($<H^2>$) of the spectrum. The central line width (ΔH_{pp}) of the nitroxide line-shape

is a common measure of nitroxide mobility. The lineshape narrows (and consequently ΔH_{pp} decreases) as the mobility of the spin label increases because the anisotropy of the g tensor (at X band) is motionally averaged. Changes in the central line width reflect changes in both the rate of the motions and the average angular fluctuations around the director axis.

Power Saturation Theory

One of the features of spin labeled proteins that can be measured by continuous wave (cw) EPR is the Heisenberg exchange rate with paramagnetic reagents. Heisenberg exchange is interpreted as a measure of solvent accessibility because it occurs when the nitroxide label comes into direct contact with paramagnetic reagents. This physical collision results in a "superexchange" interaction between spins called Heisenberg exchange, and the Heisenberg exchange rate, W_{ex}, is related to the exposure of the nitroxide to the solvent containing that reagent. Heisenberg exchange between two paramagnets provides an additional relaxation pathway for the nitroxide, and this relaxation enhancement results in faster relaxation rates. Furthermore, the nitroxide/reagent interaction must result in only Heisenberg exchange and have very little through space dipole interactions. Reagents that meet this requirement have longitudinal relaxation times much shorter than the lifetime of the nitroxide/reagent collision ($T_{1R} < \tau_c$). The longitudinal relaxation time (T_1), also called spin-lattice relaxation time, is the constant describing the decay of the spin magnetization in the z-axis towards equilibrium. More detail about T_1 and T_2 (spin-spin relaxation time) can be found in the pulsed EPR section. Heisenberg exchange rates for spin labeled proteins can be measured using cw EPR power saturation experiments. Changes in the relaxation properties of the nitroxide in the presence and absence of paramagnetic reagent are analyzed to determine an "accessibility parameter", Π, which is directly proportional to W_{ex} (*60*).

Power saturation experiments can be performed on both soluble proteins and membrane proteins. For soluble proteins, the experiment is performed by preparing two samples: one contains spin labeled protein in an appropriate buffer (for nitrogen and oxygen measurements), and the other contains spin labeled protein in the same buffer, but with the addition of the metal complex, typically 20 to 50 mM final concentration of metal reagent (purged with nitrogen). Experiments for membrane proteins are set up the same way as for soluble proteins with the only difference being the presence of lipid vesicles. Transmembrane proteins are reconstituted into vesicles whereas membrane binding proteins are mixed with vesicles. The samples are placed in gas-permeable TPX capillaries (Molecular Specialties, Inc. Catalog No. TPX-2 and TPX holder TPX H-2), equilibrated in the appropriate atmosphere and spectra acquired with the amplitude (A_{pp}) of the peak-to-peak first-derivative central resonance (m_I=0) recorded as a function of microwave power (Figure 2-4). The amplitudes are fit to the following expression to obtain a $P_{1/2}$ value (Equation 2-3).

$$A_{pp}(0) = I\sqrt{P}\left[1+\left(2^{-\varepsilon}-1\right)\frac{P}{P_{1/2}}\right]^{-\varepsilon} \tag{2-3}$$

In this equation, P is microwave power, I is a scaling factor, ε is a measure of the homogeneity of the resonance saturation, and $P_{1/2}$ is the power at which the intensity of the central line is half of its unsaturated intensity(*52*). Homogenous and inhomogeneous saturation limits have ε values ranging from 1.5 and 0.5, respectively (*60*). In this expression, I, ε, and $P_{1/2}$ are adjustable parameters and the characteristic $P_{1/2}$ value is obtained under three conditions: (1) the sample is equilibrated in diamagnetic nitrogen background, (2) equilibrated in paramagnetic air/oxygen background, where the non-polar oxygen concentrates within the bilayer or hydrophobic pockets of proteins, and (3) equilibrated in nitrogen with a water soluble metal

collider such as NiEDDA (nickel(II) ethylenediamine, *N,N'*, diacetic acid), NiAcAc (nickel(II) acetylacetonate hydrate) or CrOx (Chromium (III) oxalate) complex. In the case of nitrogen background and no paramagnetic collider, the saturation of spin labels attached to proteins is generally found to be homogeneous based on the value of $\varepsilon(60)$. The $P_{1/2}$ parameter is related to T_1 and T_2 (Equation 2-4).

$$P_{1/2} = \left(\frac{2^{2/3} - 1}{\Lambda^2 \gamma^2 T_{1e} T_{2e}} \right) \tag{2-4}$$

In most cases, $W_{ex} << 1/T_{2e}$, so T_{2e} can be treated as a constant, and

$$\Delta P_{1/2} = P_{1/2} - P^0_{1/2} = \left(\frac{2^{2/3} - 1}{\Lambda^2 \gamma^2} \right) \left(\frac{1}{T_{2e}} \right) \left(\frac{1}{T_{1e}} - \frac{1}{T^0_{1e}} \right)$$

$$= \left(\frac{2^{2/3} - 1}{\Lambda^2 \gamma^2 T_{2e}} \right) (W_{ex}) \tag{2-5}$$

Here, $P_{1/2}$ and $P^0_{1/2}$ are the power saturation parameters in the presence and absence of a paramagnetic collider, respectively, and T_{1e} and T^0_{1e} are the corresponding electron relaxation times. $\Delta P_{1/2}$ values are calculated for samples in the presence of oxygen and in the presence of aqueous metal. From the $\Delta P_{1/2}$ values, the "collision" or "accessibility" parameter, Π, for oxygen and NiEDDA can be calculated (Equation 2-6). Equation 2-6 shows the calculation of Π^{OXY} but is repeated for calculation of Π^{metal}.

$$\Pi^{oxy} \equiv \frac{\Delta P'_{1/2}(O_2)}{P'_{1/2}(DPPH)} = \frac{P_{1/2}(O_2)/\Delta H_{pp}(O_2) - P_{1/2}(N_2)/\Delta H_{pp}(N_2)}{P_{1/2}(DPPH)/\Delta H_{pp}(DPPH)} \tag{2-6}$$

The $\Delta P'_{1.2}$ value is obtained by dividing $\Delta P_{1/2}$ by ΔH_{pp}, the peak-to-peak line width of the central resonance, which normalizes the T_2 effect of the nitroxide. Π is a dimensionless quality that is normalized against a standard DPPH sample ($[P_{1/2}/DH_{pp}]_{reference}$) to account for variations in resonator efficiency for different spectrometers. Values for $P_{1/2}$(DPPH) and ΔH_{pp}(DPPH) can

be measured on dilute solid samples of DPPH (α,α'-diphenyl-β-picrylhydrazyl) in KCl. Π is proportional to the Heisenberg exchange rate (Equation 2-7).

$$\Pi = \alpha W_{ex} \tag{2-7}$$

Here, α is a constant, and W_{ex} is the Heisenberg exchange rate.

As stated earlier, Heisenberg exchange rates are interpreted as accessibility of the nitroxide to a paramagnetic reagent. For the case of membrane proteins, measuring the accessibility of nitroxides can provide a means for determining the position and/or orientation of the protein on or within lipid bilayers. This task is accomplished by defining a depth parameter, Φ, which is the natural logarithm of ratio of Π values obtained for lipid-soluble oxygen and aqueous metal complex (*52*). The Φ value is defined by the natural logarithm of the ratio of Π values (Equation 2-8).

$$\Phi = \ln\left[\frac{\Pi^{oxy}}{\Pi^{NiEDDA}}\right] \tag{2-8}$$

Φ values were related to distances from the phosphate group of lipids into the bilayer interior by determining Φ for spin labeled phosphatidylcholine lipids and for spin labeled bacteriorhodopsin (bR) mutants at known positions within the bilayer. This work shows that Φ has a relatively linear dependence as a function of depth within the bilayer (*52, 61*).

Practical Concerns

When designing power saturation experiments, the following points should be carefully considered.

Removal of histidine tags

Histidine tags are commonly used in purification of recombinant proteins because of their convenient affinity to bind columns charged with nickel. The water soluble collision reagents are

usually nickel(II) complexes, so the His-tags will sequester NiEDDA or NiAcAc and can result in falsely large values of $P_{1/2}$ if the spin label resides near the His-tag. Histidine tags are expressed on either the N- or C- termini of the protein and contain a short sequence of amino acids that is recognized by an enzyme for removal of the histidine tag.

Limitation of the power saturation method

Some spin labeled sites will not show changes in $(T_1T_2)^{-1}$ in the presence of a paramagnetic collider. Most often, this situation arises when other forms of spin-spin processes are dominant, such as in proteins that form a homodimer resulting in the spin labels placed at the dimer interface. This conformation positions two spin labels (one on each dimer) in close proximity to each other, and their spins will couple through either dipolar interactions or through Heisenberg exchange. Power saturation measures relaxation enhancement, so if the spin label is in a location where its relaxation rate is already enhanced, then power saturation can not be performed reliably *for that site*.

NiEDDA and Niacac concentrations

The final concentrations of NiEDDA or Niacac must be the same from sample to sample. Solid NiEDDA (Altenbach, PNAS, 1994) or Niacac (purchased from Aldrich) is usually dissolved in water (or the chosen buffer for experiments) to make a concentrated stock solution (10X or 100X), and a volume of this stock is mixed with buffer for rehydrating lipids. The best way to ensure that the concentrations of nickel complex remains constant is to measure the UV absorption spectrum from 200 to 800 nm of the stock solution, and to match the absorbance at λ max of each stock solution every time a new one is made.

Paramagnetic Colliders

The paramagnetic collision reagents have several important properties that make them useful for power saturation experiments. First, and most important for membrane proteins,

oxygen and the water-soluble reagents differ in polarity and therefore concentrate in the different phases of the water-bilayer system. This property is taken advantage of when distinguishing between collisions of spin labels located in solution versus within the bilayer. Water-soluble reagents should be designed to have high solubility in water and low solubility within the bilayer interior, a neutral charge, limited accessibility to the interior of a well packed protein, and be on the order of the size of the nitroxide (*60*). Having a neutral collider is important because the collision frequency is concentration dependent; therefore, electrostatic attraction or repulsion of charged complexes to charged portions of a protein might alter local concentrations of the collider and thus will skew results and lead to potentially false conclusions. The most commonly used water-soluble colliders are NiEDDA (nickel(II) ethylenediamine, *N,N'*, diacetic acid) and NiACAC (nickel(II) acetylacetonate hydrate). Either NiEDDA or NiACAC can be used for experiments conducted at neutral pH, however NiEDDA should be used for low or high pH experiments because NiEDDA remains neutral while NiACAC becomes positively or negatively charged at low or high pH, respectively. Although these two nickel complexes are more common, the anionic potassium chromium(III) oxalate (CrOx) complex has also been used for power saturation (*62*). Finally, the last point is considering the oxygen solubilization in the hydrophobic interior of lipid bilayers. The depth parameter, Φ, has been used to calibrate $P_{1/2}$ values to distances from the phospholipid head group within the bilayer interior. In an air/oxygen background, oxygen will concentrate in the hydrocarbon phase of the bilayer, and the concentration of oxygen follows a gradient with the highest amount at the center of the bilayer and the lowest amount at the lipid-water interface.

Until recently, the use of power saturation EPR for studying positions of proteins in bilayers was limited to transmembrane proteins because Φ behaves roughly linearly with

distance within bilayer interiors. Because Φ deviates from its linear behavior at distances off of the membrane surface, it fails to provide useful distance information from the membrane interface into solution, which would be useful for studying membrane binding proteins. This limitation has been overcome by incorporation of the nickel chelating lipid DOGS-NTA-Nickel into the traditional power saturation experiments. Now, instead of using any of the aqueous metal complexes, the nickel collider is localized to the bilayer and thereby provides a means for measuring collision events only for membrane bound protein. The structure of DOGS-NTA-Ni (obtained from www.avantilipids.com) is shown in Figure 2-5.

Use of DOGS-NTA-Ni in power saturation experiments is advantageous for studying soluble proteins that bind to lipid bilayers, or membrane proteins that also extend into solution, for example. The power saturation experiment proceeds as described, where the peak-to-peak amplitude is measured as a function of microwave power and data are plotted to obtain $P_{1/2}$. Also as before, two samples are prepared: one sample contains spin labeled protein with lipid vesicles (for nitrogen and oxygen measurements), and the other sample is protein with vesicles containing 10 mol% DOGS-NTA-Ni (in nitrogen background). Because collision values from DOGS-NTA-Ni can not be normalized against DPPH for calculating Π, the data are simply analyzed to obtain $\Delta P_{1/2}^{DOGS}$ by subtraction of $P_{1/2}^{Nitrogen}$ from the $P_{1/2}^{DOGS}$.

$$\Delta P_{1/2}^{DOGS} = P_{1/2}^{DOGS} - P_{1/2}^{Nitrogen} \tag{2-9}$$

Other uses of the DOGS-NTA-Ni lipid include binding proteins containing histidine tags to vesicles through coordination of the histidines to the NTA-Ni group. This strategy can be used to mimic post translational modifications of proteins, like myristoylation, which serve to anchor proteins or peptides to the bilayer surface. Additionally, binding small peptides to vesicles in this way can slow the overall correlation time of the peptide for fluorescence, NMR or EPR

experiments. This strategy can also be utilized in surface monolayer studies by SPR or other surface techniques.

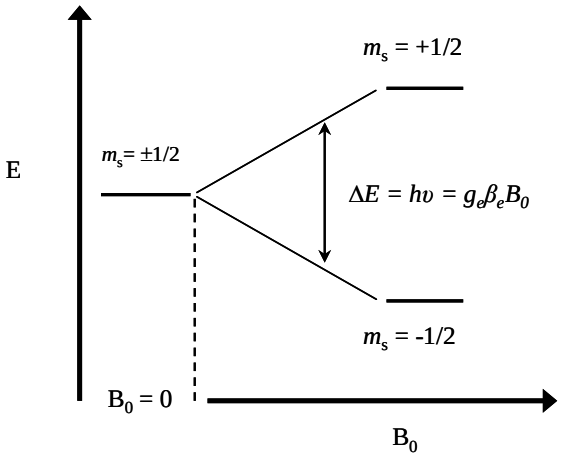

Figure 2-1. Energy level diagram for a free electron in an applied magnetic field showing the Zeeman interaction.

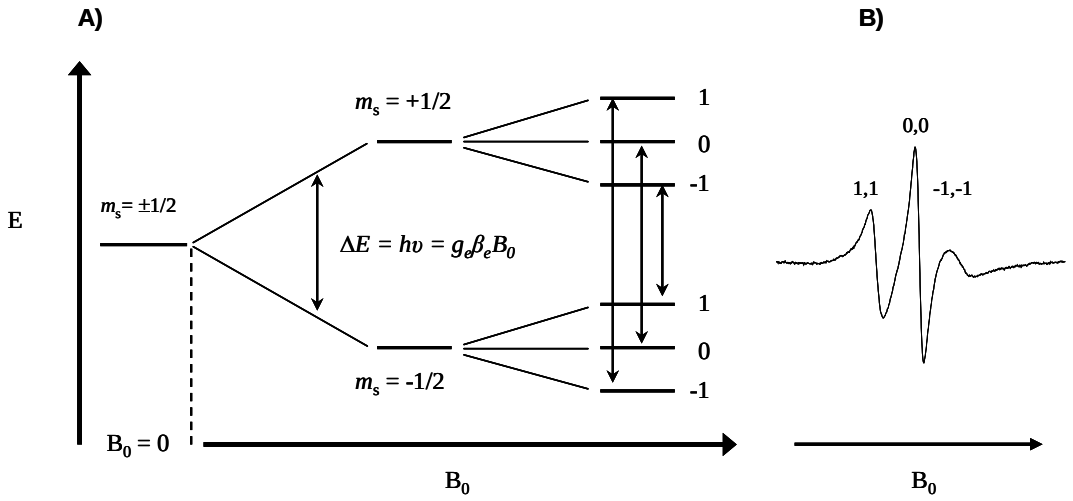

Figure 2-2. Energy diagram showing the hyperfine splitting of an electron coupled to an I=1 nucleus and the corresponding EPR line shape with three transitions. A) Hyperfine interaction diagram for a system with M_s=1/2 and M_I=1. B) EPR line shape corresponding to a system with M_s=1/2 and M_I=1. Transitions between the (M_s, M_I) states are labeled in both the energy level diagram and the resultant X-band EPR derivative spectrum. The EPR spectrum spans 100G.

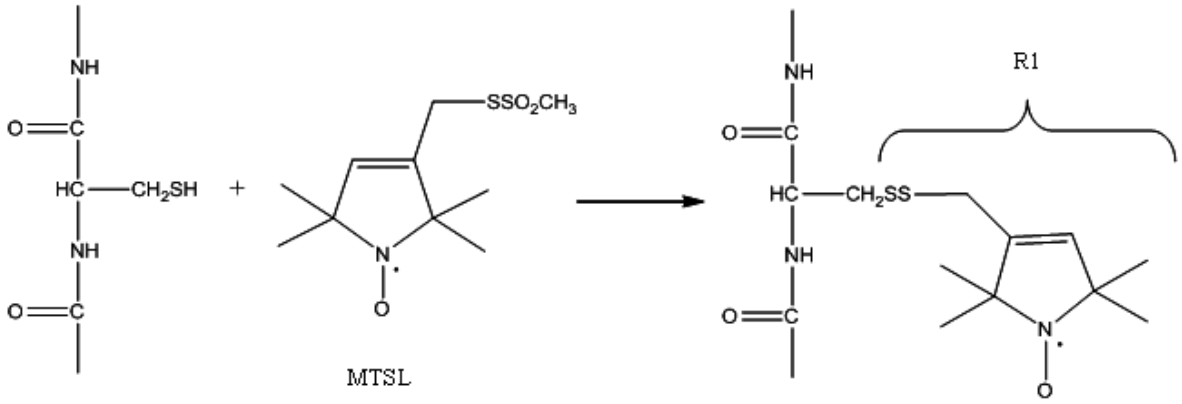

Figure 2-3. Site directed spin labeling scheme. Proteins containing cysteine mutations react with methanethiosulfonate (MTSL) spin label to form a modified side chain called R1. Covalent attachment of spin labels to proteins provides a means for using electron paramagnetic resonance spectroscopy (EPR) to study proteins that do not contain unpaired electrons.

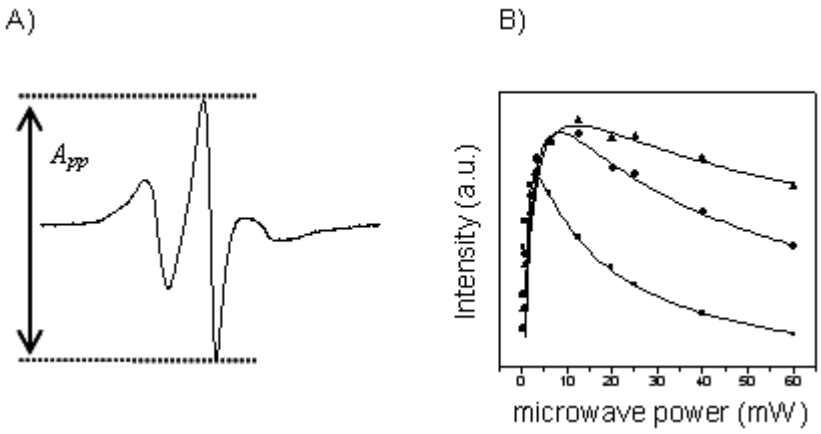

Figure 2-4. Plot showing the peak-to-peak intensity of the central resonance and the corresponding power saturation curves. A) CW X-band EPR spectrum of a nitroxide labeled protein showing amplitude (A_{pp}) of the central line. B) Plots of A_{pp} as a function of microwave power under the three experimental conditions: nitrogen (squares), air (circles), and NiEDDA (triangles). Solid lines represent the best fit to Equation 2-3 to obtain a $P_{1/2}$ values. Example $P_{1/2}$ values corresponding to these three conditions: nitrogen (squares) = 2.83, air (circles) = 8.22, and NiEDDA (triangles) = 10.51.

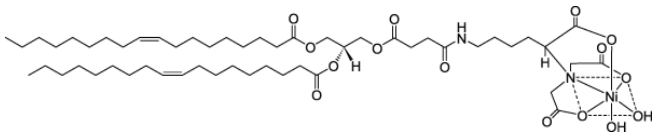

Figure 2-5. Structure of DOGS-NTA-Ni lipid (obtained from www.avantilipids.com).

CHAPTER 3
MEMBRANE BOUND ORIENTATION OF GM2AP ON POPC BILAYERS

Introduction

Gangliosides are sialic acid containing glycosphingolipids that are found in elevated concentrations in the outer membrane of neuronal cells, which function as cell markers, binding sites for viruses and bacterial toxins, and coreceptors for various hormones, as examples (*1*). Catabolism of gangliosides is a vital cellular process that occurs in the lysosomal compartments of cells where the sequential cleavage of terminal sugar residues proceeds via enzymatic degradation by more than ten different exohydrolases resulting in the production of ceramide. Upon removal of the fatty acid chain by acid ceramidase, ceramide is further degraded to sphingosine (*2*). The degradation of gangliosides that contain four or fewer sugar groups by exohydrolases requires the assistance of sphingolipid activator proteins (SAPs) (*12*). SAPs A – D and the GM2 Activator Protein (GM2AP) are the five known accessory proteins involved in ganglioside catabolism (*2*). Genetic mutations resulting in exohydrolase or accessory protein inactivity cause a number of deadly lysosomal storage diseases, including Tay Sachs disease (*1*).

GM2AP is the accessory protein required as a cofactor for the effective hydrolysis of GM2 to GM3. Fürst and Sandhoff proposed two possible *in vivo* modes by which the exohydrolase β-hexosaminidase A (Hex A) degrades GM2 in the presence of GM2AP(*63*). GM2AP binds to membrane-bound GM2 and either extracts GM2 from the bilayer, forming a protein:lipid complex in solution for proper orientation of the terminal GalNAc sugar for cleavage by Hex A to generate GM3, or GM2AP simply lifts GM2 out of the bilayer a few angstroms and hydrolysis by Hex A occurs at the bilayer surface. It is known that *in vitro*, GM2AP can bind and extract GM2 from micelles and from vesicles, forming a 1:1 complex in solution (*35*). In addition to stimulating GM2 degradation, GM2AP has also been shown to bind and transfer nonspecific

glycolipids, phospholipids (*35, Mahuran, 1998 #11, Rigat, 1997 #12*) and a fluorescently labeled dansyl lipid between vesicles (*36*). Whether transferring specific or non-specific ligands, a model for this process must include the partitioning of GM2AP with the bilayer surface. In fact, we have recently determined that GM2AP establishes a bilayer partitioning where 15% of the protein remains on the bilayer surface with 85% in solution, mostly as a protein:lipid complex (*64*). Figure 3-1 depicts this model where GM2AP establishes a series of equilibria, with the first being the binding equilibrium with lipid vesicles (K_1) where the protein recognizes either specific or non-specific lipid (K_3), which then undergoes an equilibrium dissociation ($1/K_2$) from the vesicle surface as a protein:lipid complex. Details of the molecular mechanism by which GM2AP extracts lipids from bilayers are still not well understood. It is postulated from the details of the crystal structures of GM2AP that an apolar loop spanning residues V59 – W63 (highlighted in grey in Fig 3-2 A) inserts into the bilayer upon binding to lipid bilayers (*31*). However, monolayer studies indicate that GM2AP is only surface associated to phosphatidylcholine bilayers and does not penetrate deeply into the bilayer (*65*). By determining the membrane bound orientation of GM2AP, which includes identifying those residues that interact with the bilayer, we can gain insight into the mechanism of lipid extraction.

Site directed spin labeling (SDSL) electron paramagnetic resonance (EPR) spectroscopy has become a very powerful tool for studying both soluble and membrane proteins (*48, 52, 53, 57, 61, 66-68*). In this method, site specific amino acids of the protein are individually mutated to cysteine residues to which a nitroxide spin label is attached. Here, the spin label MTSL, which attaches to cysteines through a disulfide linkage and produces the modified side chain referred to as R1, has been used and the linkage scheme is shown in Figure 3-2B. Power saturation is an EPR based technique that has been utilized for determining the relative location of a spin label

within lipid bilayers(*52*), studying accessibility of protein side chains to aqueous and lipid soluble paramagnetic colliders(*56, 57, 69*), determining conformational changes of integral membrane proteins (*70, 71*) and determining orientations of proteins on or within bilayers (*54, 61, 72*). Within this method, paramagnetic colliders of differing solubilities in the polar and nonpolar phases are utilized for discriminating the location of a spin label, where changes in the measured relaxation properties of the spin label correlate with collision frequency between the spin label and the paramagnetic collider (*52*). Examples of proteins whose orientations on bilayer surfaces have been characterized with the power saturation methodology include the C2 domains of cPLA2 and Synaptotagmin (*53, 61, 67*) and the human group IIA phospholipase A_2 (*72*).

Here, power saturation SDSL EPR spectroscopy is utilized to characterize, at low resolution, the orientation of GM2AP on phosphatidylcholine bilayer surfaces. A series of six single cysteine mutants of GM2AP were generated, the proteins expressed, purified and spin labeled. The locations of the mutations in GM2AP are shown in Figure 3-2A. Because GM2AP binds to lipid vesicles and extracts non-specific lipids, equilibrium is established where only a small fraction of the proteins remains on the bilayer surface. Hence, the traditional use of water soluble paramagnetic colliders such as NiEDDA or Niacac cannot be used for determining the orientation of the membrane bound state. Instead, a variation of the traditional power saturation method was employed, which utilizes the nickel chelating lipid (DOGS-NTA-Ni), which provides a surface bound paramagnetic collider. With this method, relaxation induced by only the surface bound state is detected, so those sites that collided with the DOGS-NTA-Ni can be mapped onto the crystal structure, thereby providing a low resolution model for how GM2AP orients on the POPC bilayer surface. These results show that GM2AP binds such that the entire face of the protein containing the lipid binding pocket lies onto the bilayer surface. This

orientation differs from that proposed from the X-ray structure but is consistent with other models of lipid binding proteins, including Sec14p (*73, 74*).

Materials and Methods

Materials

1-palmitoyl-2-oleoyl-sn-glycero-3-phosphocholine (POPC) in chloroform, bis(monooleoylglycero)phosphate (BMPdi18:1 or DOBMP) in chloroform, and 1,2-dioleoyl-sn-glycero-3-[(N-(5-amino-1-carboxypentyl)iminodiacetic acid)succinyl] (Nickel salt, in chloroform) (DOGS-NTA-Ni) were purchased from Avanti Polar Lipids (Alabaster, AL) and used without further purification. N-(5-dimethylaminonaphthalene-1- sulfonyl)-1,2-dihexadecanoyl-sn- glycero-3-phosphoethanolamine, triethylammonium salt (DDHPE) was purchased from Molecular Probes (Eugene, OR) in the form of powder. Methanethiosulfonate spin label (MTSL) was purchased from Toronto Research Chemicals, Inc. Unless otherwise stated, all other reagents were from Fisher Scientific and used as received.

Protein Expression and Purification of GM2AP Mutants

Recombinant GM2AP WT and cysteine mutant constructs prepared using an *E. coli* expression system as described in an earlier report (*36*) and was a modified procedure originally published by Wright (*31*). Spin labeling of GM2AP cysteine mutants proceeded after the refolding step by buffer exchanging by dialysis into 25 mM Tris, 2.5% glycerol, 0.05% Tween 20, pH 6.8 buffer and then adding approximately 100x molar excess MTSL dissolved in a minimal amount of ethanol. The labeling reaction proceeded in the dark at 4°C overnight. WT GM2AP does not label. Removal of excess spin label with concurrent pH adjustment for anion exchange proceeded by dialyzing the sample against 25 mM Tris, 2.5% glycerol, 0.05% Tween 20, pH 8 buffer. The protein was concentrated by anion exchange chromatography (Q column) and eluted with 0.5 M NaCl (25 mM Tris, 2.5% glycerol, 0.05% Tween 20, 250 mM NaCl, pH

8.0) buffer. Protein was determined to be > 95% pure after Q column by SDS PAGE. Gel filtration using a Sephacryl S200 column was required to separate properly folded protein from aggregated and misfolded protein and to remove the detergent Tween 20 that was in several of the previous purification buffers. The column was equilibrated and protein was eluted in 50 mM sodium phosphate, 150 mM NaCl, 2.5% glycerol, pH 7 buffer. Protein was stored in the 50 mM sodium phosphate, 150 mM NaCl, 2.5% glycerol, pH 7 buffer at -20°C.

CD Measurements

CD spectra were measured with an Aviv-400 Spectropolarimeter at 25ºC using a 1 mm pathlength cuvette. Data were collected from 260 nm to 190 nm every 1 nm with a 1 nm bandwidth**.** Each sample was measured twice and the two scans were averaged. CD spectra of WT and cysteine mutant constructs of GM2AP were measured for protein concentrations ranging from 50 μM to 80 μM in 50 mM phosphate, 150 mM NaCl, 2.5% glycerol pH 7.0 buffer.

Preparation of POPC:Dansyl-DHPE Liposomes

POPC in chloroform was purchased from Avanti Polar Lipids (Alabaster, AL) and used without further purification. Dansyl-DHPE (DDHPE) was obtained from Molecular Probes (Eugene, OR) in the form of powder. R18 was obtained from Molecular Probes (Eugene, OR) in the form of powder. POPC:DDHPE (4:1 in molar ratio) vesicles were prepared by mixing the desired amounts of both lipids (in chloroform), drying to a film by a stream of nitrogen and vacuum desiccation for 6-12 hours. For kinetic measurements, the dried lipid films were hydrated for one hour in an appropriate volume of 50 mM sodium acetate buffer, pH 4.8. Large unilamellar vesicles (LUVs) of above lipid samples were prepared by extrusion through 100 nm polycarbonate filters with 55 passes using a hand-held miniextruder (Avanti, Alabaster, AL).

Final phospholipid concentrations were determined on the basis of total phosphate determination by Malachite Green Phosphate Assay Kit (BioAssay Systems).

Dansyl Extraction Functional Assay

An assay to characterize the function of the CYS-spin labeled GM2AP constructs was developed. Here, function is defined as ability of GM2AP to bind to lipid vesicles and extract DDHPE to form a GM2AP:DDHPE complex in solution. The formation of the complex is followed with fluorescence spectroscopy using a dansyl-fluorescence based lipid extraction assay recently reported (*36*). Fluorescence spectra were acquired with a FluoroMax-3 fluorometer (Jobin Yvon Horiba, NJ) with a 4 mm light path quartz cuvette (Starna, Atascadero, CA) controlled to 20º C with HAAKE K20 temperature controller (Thermo Electron Corporation, Waltham, MA). For all measurements, the excitation wavelength was set to 340 nm, with excitation and emission slits set to 2 nm and 5 nm, respectively. For lipid extraction experiments, the light scattering due to high concentrations of lipid vesicles was reduced by setting the excitation and emission polarizers to 90º and 0 º orientations, respectively (*75*). 5 μM final GM2AP concentration was allowed to equilibrate with POPC:DDHPE (4:1) vesicles (1 μM final lipid concentration) in 50 mM sodium acetate pH 4.8 buffer. Spectral scans from 470 nm to 530 nm were collected every 15 seconds for the first 1.5 minutes and then every 30 seconds. Extraction of DDHPE was evidenced by a blue shift of emission from 518 nm (in bilayer) to 484 nm (protein bound) (*36*). The half– life ($t_{1/2}$) of dansyl extraction was determined by plotting the fluorescence intensity at 484 nm as a function of time and fitting the curve to a first order exponential, where

$$A = A_0 e^{-kt} \tag{3-1}$$

and the half-life for a first order exponential decay is

$$t_{1/2} = \frac{\ln 2}{k} \tag{3-2}$$

Quantification of GM2 Extraction

GM2 extraction was quantified with an absorption resorcinol assay (*76*). For these experiments, 7.5 nmol GM2AP and 200 nmol vesicles containing 10 mol% GM2 with POPC, were mixed in NaOAc buffer (50 mM, pH 4.8) with total volume of 100 μL and incubated 20 min at room temperature. Then the mixture was loaded onto a self-packed column (1.6x500 mm) with sephacryl S-200. The elution fractions were collected every 2 drops. The fraction volume was determined by weight or micro syringe to be on average 45 μL in our experiments. For fractions not containing vesicles, GM2AP concentration was determined from the optical density at 280 nm (OD_{280}) with a 1 cm light path microcell. The GM2 concentration in each fraction (with or without vesicles) measured by the resorcinol assay (*76*) where the total volume of the fraction was mixed with equal volume (45 μL) of freshly prepared resorcinol reagent in a 250 μL centrifuge tube. 10 mL resorcinol reagent contains: 8 mL concentrated hydrochloric acid, 1 mL 2% resorcinol, 25 μL of 100 mM copper sulphate and 975 μL water. The mixture was incubated in a boiling water bath for 15 minutes. After heating, the tubes were cooled in running water. 60 μL of n-butyl acetate:n-butanol (85:15 by volume) was added to each tube. The tubes were shaken vigorously and placed in ice water for 15 minutes. The mixture was then spun at 4000 rpm 2 minutes on benchtop centrifuge (Beckman, Fullerton, CA) to separate solvent phase. The OD_{580} nm of the organic solvent phase was measured for concentration determination. The extinction coefficient of the complex formed by GM2 with resorcinol was acquired from two methods. First, the extinction coefficient was directly measured with purchased GM2 (1 mg per vial), which gives an extinction coefficient of 5700 $mol^{-1}cm^{-1}$. In addition, a standard curve was generated using N-acetylneuraminic instead of GM2 due to its relative expense. From the best fit

line, an extinction coefficient for the N-acetylneuraminic acid-resorcinol complex was obtained. According to references, this value can be divided by 0.77 to give an estimated extinction coefficient for resorcinol complexes with gangliosides. Following this method, we obtained a value of 5600 $mol^{-1}cm^{-1}$, which is very close to the value obtained directly for a solution of GM2.

CW-EPR Solution Data Collection

Continuous wave EPR spectra were collected on a modified Bruker ER200 spectrometer with an ER023M signal channel, an ER032M field control unit and equipped with a loop gap resonator (Medical Advances, Milwaulkee, WI). Solution spectra of GM2AP mutants were recorded with protein samples in sealed round capillaries, 0.60 mm x 0.84 mm x 100 mm (Fiber Optics Center, Inc.; New Bedford, MA), at room temperature and with 3.16 mW incident power. Concentrations of protein ranged from 100-200 μM in either 50 mM Tris pH 8.0 or 50 mM NH_4Ac pH 4.5 buffers. Labview software was used for baseline correction, free spin subtraction (when applicable) and double integral area normalization, and was generously provided by Drs. Christian Altenbach and Wayne Hubbell (UCLA).

Preparation of Lipid Vesicles

Lipid vesicles comprised of POPC, POPC:DOGS-NTA-Ni (9:1 molar ratio), and POPC:DDHPE (4:1 molar ratio) were prepared by mixing appropriate volumes of stock solution of POPC, DOGS-NTA-Ni, or DDHPE in chloroform, removing the organic solvent by drying under nitrogen stream and vacuum-desiccating overnight. Two separate samples of POPC LUVs were prepared. The first was rehydrated in 50 mM ammonium acetate (NH4Ac) pH 4.5 buffer, and the second was rehydrated in 50 mM NH4Ac pH 4.5 buffer containing 50 mM final concentration of NiEDDA. POPC:DOGS-NTA-Ni (9:1) lipid films were rehydrated by vortexing in 50 mM NH4Ac pH 4.5 buffer; POPC:DDHPE (4:1) lipids were rehydrated by vortexing in 50

mM sodium acetate pH 4.8 buffer. For all samples, rehydration proceeded for 15 minutes at room temperature with gentle vortex mixing. Large unilamellar vesicles (LUVs) of the above lipid samples were prepared by extrusion consisting of 55 passes through 100 nm polycarbonate filters using an Avanti hand-held miniextruder (Alabaster, AL). Stock solutions of POPC and POPC:DOGS-NTA-Ni (9:1) LUVs were prepared at 200 mM. Final lipid concentrations for power saturation experiments were 20 mM total lipid. For those samples containing NiEDDA, the final concentration of NiEDDA was 20 mM.

Power Saturation EPR Experiments

Two different sets of power saturation experiments are presented in this work: (1) the traditional power saturation experiment utilizing oxygen and NiEDDA colliders and (2) power saturation using DOGS-NTA-Ni lipid as the paramagnetic collider. Traditional power saturation experiments were collected at both pH 4.5, where GM2AP binds to lipid vesicles, and at pH 8.0, where GM2AP is unbound (*64*). Spin labeled GM2AP mutants in 50 mM NH_4Ac pH 4.5 buffer or 50 mM Tris pH 8.0 buffer were mixed with POPC LUVs (50 mM NH_4Ac pH 4.5) or with POPC LUVs in 50 mM NH_4Ac pH 4.5 containing a final concentration of 20 mM NiEDDA. Final concentrations of protein and lipid were 120 μM and 20 mM; respectively. For pH 8.0 samples, the stock concentrations of protein (pH 8.0) and lipid (pH 4.5) were such that the sample after mixing protein with lipid was pH > 7, which is sufficient for GM2AP to remain unbound. EPR spectra were collected from samples placed in gas-permeable TPX capillary tubes (Molecular Specialties Medical Advances, Milwaulkee, WI) and equilibrated with either nitrogen gas or air (20% oxygen). The peak-to-peak first derivative amplitude, A_{pp}, of the central resonance ($m_I = 0$) was measured and plotted as a function of microwave power, P, ranging from incident power of 0.2 – 63 mW. The resultant curves were fit to the expression

$$A_{pp}(0) = I\sqrt{P}\left[1+\left(2^{-\varepsilon}-1\right)\frac{P}{P_{1/2}}\right]^{-\varepsilon} \tag{3-3}$$

where I is a scaling factor, $P_{1/2}$ is the power at which the resonance amplitude is one half its unsaturated value, and ε is a measure of the homogeneity of the saturation of the resonance (*52*). $P_{1/2}$ values were obtained under three different sample conditions for samples at both pH 4.5 and pH 8.0 (a total of six power saturation experiments): a) protein mixed with POPC LUVs equilibrated in nitrogen gas, b) protein mixed with POPC LUVs equilibrated in lipid soluble air (20% oxygen), and c) protein mixed with POPC LUVs with aqueous soluble 20 mM NiEDDA equilibrated in nitrogen. $\Delta P_{1/2}$ values were obtained by subtracting the $P_{1/2}$ value for nitrogen from the $P_{1/2}$ values of oxygen and NiEDDA. Collision parameters, Π, for oxygen and NiEDDA were calculated according to Equation 3-4.

$$\Pi^{Oxy} \equiv \frac{\Delta P_{1/2}^{'}(Oxy)}{P_{1/2}^{'}(DPPH)} = \frac{P_{1/2}(Oxy)/\Delta H_{pp}(Oxy) - P_{1/2}(N_2)/\Delta H_{pp}(N_2)}{P_{1/2}(DPPH_2)/\Delta H_{pp}(DPPH_2)} \tag{3-4}$$

Π values for NiEDDA were calculated by substituting $P_{1/2}$(NiEDDA) for $P_{1/2}$(Oxy) in Equation 3-4.

A separate set of power saturation experiments utilizing DOGS-NTA-Ni as the paramagnetic collider were also performed under the following three conditions: pH 4.5, pH 4.5 + EDTA and pH 8.0 (all under a nitrogen atmosphere). Spin labeled GM2AP mutants in 50 mM NH_4Ac pH 4.5 buffer or 50 mM Tris pH 8.0 buffer were mixed with POPC:DOGS-NTA-Ni (9:1) LUVs in 50 mM NH_4Ac pH 4.5 buffer to give final protein and lipid concentrations of 120 μM and 20 mM, respectively. Two additional samples were also prepared for measuring the relaxation properties of each spin labeled site in absence of collider that contained GM2AP mutants in both pH 4.5 and pH 8 buffers with POPC LUVs in 50 mM NH_4Ac pH 4.5 buffer.

Final protein and lipid concentrations were as described above. $P_{1/2}$ values (Equation 3-3) were measured for GM2AP mutants mixed with POPC:DOGS-NTA-Ni (9:1) LUVs and for GM2AP mutants with POPC LUVs. $\Delta P_{1/2}$ values were obtained by subtracting the $P_{1/2}$ value for GM2AP with POPC in nitrogen from the $P_{1/2}$ values of GM2AP mutants with POPC:DOGS-NTA-Ni (*66*), and is shown in Equation 3-5.

$$\Delta P_{1/2}(\text{DOGS}) = P_{1/2}(\text{DOGS-NTA-Ni}) - P_{1/2}(\text{POPC}) \quad (3\text{-}5)$$

Power saturation data for the pH 4.5 + EDTA experiments were collected on the same samples used at pH 4.5. Here, 2 μL of 0.5 M EDTA solution was added to the 10 μL samples containing POPC:DOGS-NTA-Ni (9:1), to remove the nickel from the NTA chelator group, which is covalently attached to DOGS-NTA-Ni lipid, and the power saturation experiment was repeated with equilibration in nitrogen gas. $\Delta P_{1/2}$ values were obtained by subtracting the $P_{1/2}$ value for GM2AP with POPC in nitrogen from the $P_{1/2}$ values of GM2AP mutants with POPC:DOGS-NTA-Ni + EDTA.

DOGS-NTA-Ni Extraction

Power saturation with sucrose loaded POPC:DOGS-NTA-Ni (9:1) vesicles was performed using L126R1, which showed large collisions with DOGS-NTA-Ni. After power saturation measurements, the sucrose loaded vesicles were pelleted, the supernatant was collected and the power saturation was repeated for L126R1 in solution, presumably as a protein:lipid complex.

Sucrose loaded POPC:DOGS-NTA-Ni (9:1) vesicles were prepared by mixing appropriate volumes of POPC and DOGS-NTA-Ni (both in chloroform) in a glass tube, dried over a stream of nitrogen to produce a lipid film and vacuum dessicated overnight. The lipid mixture was rehydrated in 176 mM sucrose, 50 mM NH_4Ac pH 4.5 buffer with gentle vortexing to give a final lipid concentration of 100 mM. Large unilamellar vesicles (LUVs) were prepared by

extrusion through 100 nm polycarbonate filters with 55 passes using a hand-held miniextruder (Avanti, Alabaster, AL). L126R1 was buffer exchanged by dialysis to 100 mM KCl, 50 mM NH_4Ac pH 4.5, which is isoviscous to the sucrose buffer of the lipid sample. A 20 μL sample was prepared containing 150 μM final protein concentration and 20 mM final lipid concentration and was allowed to incubate for 20 minutes. 5 μL of sample was placed in a TPX tube and equilibrated in nitrogen background for an additional 20 minutes. Power saturation was performed and the data were fit to Equation 3-3 to obtain a $P_{1/2}$ value as described in the text. After power saturation, the 5 μL sample from the TPX tube was returned to the rest of sample, and the 20 μL sample was diluted to 200 μL final volume with 100 mM KCl 50 mM NH_4Ac pH 4.5 buffer. The unbound L126R1 in solution was separated from L126R1 bound to the sucrose loaded vesicles by pelleting using an Air-Driven Ultracentrifuge (Beckman) at a speed of 100,000 g for 1 hour. The supernatant containing unbound L126R1 (most likely as protein:lipid complex) was collected and concentrated to 150 μM. 5 μL was placed in a TPX tube and equilibrated in nitrogen gas for 20 minutes, the power saturation was repeated in solution for L126R1 and data were fit to Equation 3-3 to obtain a $P_{1/2}$ value. If L126R1 did extract DOGS-NTA-Ni and large $P_{1/2}$ values at this site resulted from collisions of the spin label with the protein-bound lipid in solution, the addition of EDTA to remove the nickel ion from the protein:lipid complex would result in a decrease in $P_{1/2}$ value. After power saturation of L126R1 in solution, 2 μL of 0.5 M EDTA was added to the sample and power saturation was repeated in nitrogen background.

Results

Six sites of GM2AP (V54C, I66C, T90C, S115C, L126C, N136C) were chosen for single amino acid substitution to cysteine for subsequent spin labeling. These spin labeled sites were

used to determine what regions of GM2AP interact with the lipid bilayer surface. The locations of these cysteine mutation sites are shown as spheres in the ribbon diagram of GM2AP in Figure 3-2. Proper folding of spin labeled GM2AP mutants was verified by circular dichroism spectroscopy (CD), where the CD spectra of spin labeled mutants were identical to published WT GM2AP (Fig 3-3). The function of GM2AP spin labeled mutant constructs, defined as the ability to extract the fluorescently labeled lipid *N*-(5-dimethylaminonaphthalene-1- sulfonyl)-1,2-dihexadecanoyl-sn-glycero-3-phosphoethanolamine (DDHPE) from POPC:DDHPE (4:1) LUVs, was assayed as described in an earlier report (*36*). Briefly, protein and lipid vesicles were mixed to give a final concentration of 5 μM GM2AP in 50 mM sodium acetate pH 4.8 buffer and 1 μM POPC:DDHPE (4:1) LUVs. Spectral scans from 470 nm to 530 nm were measured as a function of time. The fluorophore of DDHPE is attached to the polar head group of the lipid, and in lipid bilayers, DDHPE has a maximum emission wavelength of 518 nm. Upon extraction by GM2AP, the emission wavelength shifts to 484 nm when DDHPE is bound by GM2AP. The blue shift is seen because the fluorophore of DDHPE moves from a more polar environment at the lipid–aqueous interface to the hydrophobic binding pocket of GM2AP. From these experiments, the $t_{1/2}$ values for DDHPE extraction for spin labeled GM2AP constructs was compared to the value obtained for WT GM2AP. Results are given in Table 3-1. Spin labeled mutants extract DDHPE from POPC LUVs at a rate that was within error of WT with a few exceptions. V54R1 extracted DDHPE slightly faster ($t_{1/2}$ = 0.9 ± 0.1 minutes) than WT ($t_{1/2}$ = 1.5 ± 0.1 minutes), and S115R1 extracted DDHPE slower ($t_{1/2}$ = 5.16 ± 0.8 minutes) than WT. Spin labeled I66R1 exhibited no extraction of DDHPE; however, the location of this site in one of the putative binding loops that likely results in the spin label sterically blocking the lipid binding cavity. The extraction assay was repeated for I66R1 after reducing the spin label with ascorbic acid to ensure that lack of

fluorescence signal did not occur from spin label quenched fluorescence. Again, no extraction of DDHPE was detected. However, the introduction of R1 at this site (I66C) did *not* alter the extraction efficiency of GM2 from POPC LUVs (details in supplementary information). Results showed that I66R1 can extract GM2 from POPC LUVs comparable to WT. This finding can be understood based upon the two different hydrophobic binding pockets seen in X-ray crystallography of GM2 and phospholipids (*77*). For phospholipids, the head group of the lipids binds near the two flexible hydrophobic loops, which contain residue I66. On the other hand, when GM2 is bound, the sugar head group protrudes from the protein, near the alpha helix with ceramide tails contained in the upper portion of the hydrophobic pocket (*77*).

EPR spectral line shapes for the R1 labeled GM2AP CYS mutants are shown in Figure 3-4 for GM2AP in solution at neutral pH (50 mM Tris pH 8.0). Two spin labeled sites, L126R1 and N136R1, are both located in one of the two putative lipid bilayer binding loops and have EPR line shapes characteristic of spin labels in aqueous exposed flexible regions on proteins (*49*). I66R1 is located on the other putative binding loop and has a line shape with a broad component reflecting possible tertiary contact of R1 with neighboring residues around the lipid binding cleft. The broadened line shape for I66R1 also supports the argument that R1 at this site sterically interferes with DDHPE extraction. Sites V54R1 and S115R1 are located on the back side of β-strands β-4 and β-6, respectively (*31*), and their EPR line shapes are slightly broadened, consistent with the attachment of R1 to a rigid portion of the protein . The spectrum of T90R1 is the narrowest line shape observed for those sites investigated here, indicating a high degree of mobility. This mobility is not unexpected given its location in a loop structure and high B-factors observed in the X-ray structure (*31*). Each of the spin labeled sites has line shapes that are expected from comparison to the crystal structure. Interestingly, the EPR line shapes did not

change within signal to noise when POPC vesicles were added. The significance of this finding is discussed further within.

Power saturation EPR experiments were performed for each of the R1 mutants with lipid vesicles in attempts to determine a membrane bound orientation of GM2AP on POPC surfaces. Exposure of R1 to either lipid-soluble oxygen or aqueous-soluble NiEDDA results in physical collisions between R1 and the collider, and the values of the collision parameter (Π) for oxygen and NiEDDA can be calculated (*52, 61, 72*). Given that GM2AP functions at acidic pH, samples containing 20 mM POPC LUVs were prepared in 50 mM NH_4Ac pH 4.5 buffer. The lipid-to-protein ratio was approximately 160:1, which was originally intended to ensure that the protein was fully bound. However, we have demonstrated that GM2AP establishes equilibrium partioning where only 15% of the protein remains on the vesicle surface, even when POPC is used as the lipid substrate. This equilibrium pattern has been seen for a variety of lipid compositions investigated (*64*). The inability to generate a sample where > 99% of the protein is on the bilayer surface has a significant impact on the interpretation of the power saturation data. Oxygen accessibility (Π^{Oxy}) and NiEDDA accessibility (Π^{NiEDDA}) parameters were calculated from the power saturation curves for each of the six sites and the values are reported in Table 3-1. It has been shown that by plotting Π^{NiEDDA} versus Π^{Oxy}, a correlation between collision parameters with spin label location in either the aqueous or lipid phases can be obtained (*61, 78*). Sites that are known to reside within the bilayer, such as DOXYL labels in phospholipids acyl chains and spin labeled bacteriorhodopsin, cluster in one region of the graph, whereas the aqueous exposed sites of the C2 domain of cPLA2 result in values that cluster in another region. Figure 3-5 shows this correlation and also plots the collision parameters obtained for GM2AP. One site (V54R1) falls in the aqueous portion of the graph and is consistent with the given model

of a membrane bound orientation where the back side of the protein is aqueous exposed. Site L126R1 falls in the lipid portion and correlates with our model orientation which positions this site on the bilayer surface. However, the remaining data points are located outside the boundaries for each phase and are inconsistent with other data in the literature. At first this result was surprising but can be understood when considering recent results by Ran, *et al.* (*36, 64*) that showed by fluorescence and sucrose loaded vesicle experiments that GM2AP establishes an effective bilayer partitioning where approximately 15% GM2AP remains bound to the bilayer surface, regardless of lipid concentration. Because GM2AP can extract POPC and other non-specific lipids in addition to its specific ligand GM2, an equilibrium is established with free GM2AP, GM2AP bound to the lipid vesicles (either with or without GM2 ligand), and GM2AP:lipid complex in solution. From assays using POPC:DDHP with the lipid-to-protein ratios utilized for power saturation SDSL EPR measurement (160:1), equilibrium for GM2AP:DDHPE formation occurs in approximately 1.5 minutes for lipid to protein ratios used here. The reverse process is slow ($t_{1/2}$ is near 20 minutes). The EPR data were collected after waiting at least twenty minutes after mixing GM2AP with lipid vesicles. Figure 3-1 gives a graphical representation of the equilibrium binding model of GM2AP. This equilibrium of 15% bound – 85% in solution can explain why most of the data correlating collision parameters Π^{Oxy} and Π^{NiEDDA} fall outside of the defined regions of the graph. In the oxygen experiment, changes in saturation are detected for those protein molecules bound to the POPC bilayer. The values obtain for Π^{Oxy} indicate that certain sites are located near the bilayer interface. However, in the NiEDDA experiment, the Π^{NiEDDA} values are dominated by collisions with GM2AP in solution. Currently, we do not know the exchange rate of the protein on and off the bilayer, but we assume it is much slower than the ns time scale of the paramagnetic relaxation. Due to the partitioning

behavior of GM2AP, traditional power saturation experiments can not be utilized for determining an orientation on bilayer surfaces, as has been done for C2 domains.

Because GM2AP can extract POPC as a non-specific ligand from vesicles under acidic conditions, an equilibrium is established where only a small percentage of the protein remains surface associated, with a majority of GM2AP forming a soluble protein:lipid complex (*36*, *64*). Hence, a surface-bound collider was utilized to map those sites in GM2AP that come into contact with the POPC vesicle surface during binding/lipid extraction. The lipid DOGS-NTA-Ni has a linker that extends from the phosphate head group into solution a maximum of 14 Å (*66*) and contains a nickel ion coordinated by the iminodiacetate ligand. This lipid has been previously utilized to characterize surface located residues in the integral membrane protein KcsA (*66*) and to investigate the interactions of the cytoplasmic domain of phospholamban with sarcoplasmic reticulum Ca^{2+}-ATPase (*69*). Here, DOGS-NTA-Ni was incorporated into POPC bilayers (POPC:DOGS 9:1) to serve as a surface bound paramagnetic collider in the power saturation experiments such that relaxation would occur for only those sites that were interacting with the bilayer surface. $\Pi^{\text{DOGS-NTA-Ni}}$ values were determined as described in Equation 3-4. Figure 3-6 shows power saturation curves obtained for the spin labeled GM2AP mutants mixed with POPC:DOGS-NTA-Ni (9:1) LUVs purged with a nitrogen background for pH 8, pH 4.5, and pH 4.5+EDTA. Very low $\Pi^{\text{DOGS-NTA-Ni}}$ values ($\Pi < 0.1$) were seen for all spin labeled positions at pH 8 as expected, because GM2AP remains unbound at neutral pH. At pH 4.5, surface bound GM2AP molecules showed accessibility to DOGS-NTA-Ni for sites T90R1, L126R1, and N136R1, as seen by larger $\Pi^{\text{DOGS-NTA-Ni}}$ values ($\Pi > 0.1$) compared to those obtained at pH 8. Because the larger $\Pi^{\text{DOGS-NTA-Ni}}$ values result from higher frequencies of collision of the spin label with the surface-bound collider, it is evident that these three sites interact with the bilayer

surface. Sites V54R1, I66R1 and S115R1 had low $\Pi^{\text{DOGS-NTA-Ni}}$ values ($\Pi < 0.1$) at acidic pH. Although these low values can indicate that these GM2AP constructs did not bind to the LUVs, the DDHPE extraction assay for V54R1 and S115R1 confirm function; and therefore, the power saturation results are interpreted to mean that GM2AP binds to vesicles in an orientation that makes R1 at these two sites inaccessible to colliding with DOGS-NTA-Ni.

Our proposed membrane bound orientation positions I66R1 near the bilayer surface (discussed below), but R1 at I66C showed very low collision values with DOGS-NTA-Ni. This finding, along with the relatively broadened I66R1 spectral line shape and the high collisions with oxygen when power saturation was performed on protein in solution are consistent with a model where the spin label is tucked in towards the hydrophobic cavity. It is also likely that the A60 apolar loop that contains I66 is seen in an extended conformation in the crystal structure due to crystal-crystal contacts in the unit cell. High collisions to oxygen in solution can arise from local high concentrations of oxygen within the hydrophobic interior pocket of GM2AP. In addition, spin labeled I66C was unable to extract DDHPE from vesicles, a finding also consistent with the spin label tucked into the hydrophobic binding pocket, sterically blocking the opening to the cavity where non-specific ligands bind and preventing DDHPE from entering. Interestingly, although the spin label at site I66C prevents the extraction of DDHPE, we find that the I66R1 construct can extract the specific ligand of GM2AP, the ganglioside GM2, from POPC:GM2 (3:1) LUVs. Sites T90C and L126C showed the largest $\Pi^{\text{DOGS-NTA-Ni}}$ values indicating the closest contact with the bilayer. Site T90C is particularly significant because the strong collisions of R1 with DOGS-NTA-Ni at this site suggest an orientation of lipid binding that is different from the proposed conformation based upon analysis of hydrophobic regions of the protein in the X-ray structures (*30, 31, 77*). For all sites, after performing the power saturation experiment at pH 4.5,

an excess of EDTA was added to the sample to remove the nickel from the surface, and the power saturation was repeated. Removal of surface-bound collider resulted in decreased relaxation enhancement of the spin label and therefore, resulted in lower $\Pi^{\text{DOGS-NTA-Ni+EDTA}}$ values than those obtained at pH 4.5 without EDTA. For all spin labeled sites, the power saturation curves for DOGS-NTA-Ni with EDTA resembled those for unbound GM2AP (pH 8). This decrease in $\Pi^{\text{DOGS-NTA-Ni+EDTA}}$ values upon addition of EDTA confirms the protein's association with lipid bilayers.

Because GM2AP extracts lipids from LUVs, a control experiment was performed to test if GM2AP can significantly extract DOGS-NTA-Ni lipid, which contains the surface bound metal, from POPC LUVs. Extraction of DOGS-NTA-Ni from POPC vesicles to form a protein:lipid complex in solution could result in an incorrect interpretation of collision data, depending on how GM2AP binds the DOGS-NTA-Ni lipid. DOGS-NTA-Ni has a rather large polar head group, consisting of a 14 Å linker with an iminodiacetic acid group that chelates a nickel ion at the end, so it is unlikely that the hydrophobic binding pocket of GM2AP could accommodate binding DOGS-NTA-Ni in the same way as it is thought to bind DDHPE and other phospholipids, where the entire lipid is contained in within the binding pocket (*77*). GM2AP binds its specific ligand GM2 in a different manner where the acyl tails are in the pocket and the oligosaccharide head group is aqueous exposed. Given the large size of the DOGS-NTA-Ni head group, it is possible that DOGS-NTA-Ni could be oriented in the lipid binding cavity in the same way as GM2; although, this orientation is unlikely because only gangliosides have been found to bind efficiently in this manner, and ceramide has significantly weaker binding than GM1 or GM2. The text of this manuscript describes that GM2AP establishes a bilayer partitioning where 15% of the protein remains on the bilayer surface with 85% in solution, mostly as a protein:lipid

complex (*64*). These experiments were repeated twice and the $P_{1/2}$ values are listed in Table 3-2. $P_{1/2}$ values for L126R1 in solution and with EDTA are lower than values of L126R1 with vesicles. As can be seen in Table 3-2, the difference between values of $P_{1/2}$ for protein bound the the vesicles and those in the supernatant is nearly 2; wherase the change upon adding EDTA is almost 10-fold less (0.2). These results indicate that the collisions of DOGS-NTA-Ni with GM2AP do not arise from a GM2AP:DOGS-NTA-Ni complex. The slight change upon adding EDTA can arise from incomplete pelleting of lipid vesicles, as our method is known to pellet only 90-95% at the concentrations used for this assay.

We can compare $\Pi^{\text{DOGS-NTA-Ni}}$ values obtained in this study to values published for KcsA (*66*). Figure 3-7 is a plot of $(\Pi^{\text{DOGS-NTA-Ni}})^{-1}$ versus $(\Pi^{\text{Oxy}})^{-1}$ for GM2AP (solid diamonds) and for KcsA (open circles). For both GM2AP and KcsA, sites of high collisions with DOGS-NTA-Ni have similar Π values and occur at the lipid – aqueous interface where the spin labels are the most accessible to the surface bound collider. Decreased values of collision parameters are observed for spin labeled sites in KcsA that move further into the bilayer. For GM2AP, the sites with low Π values arise from an orientation of the protein on the bilayer surface that positions the spin labels so that they are unable to physically collide with DOGS-NTA-Ni, or, for the case of I66R1, where the label is tucked into the hydrophobic pocket. From mapping the relative accessibility to DOGS-NTA-Ni for various sites of GM2AP, we propose a model where GM2AP sits on the bilayer surface with the face of the hydrophobic pocket pointing towards the phospholipid interface. This orientation differs from the original hypothesized model that suggested that the protein bound to bilayers in an upright fashion so that the apolar loop inserted into the bilayer. The high collision value for T90R1 with DOGS-NTA-Ni means that this site is close to the bilayer surface, and that constraint was not accommodated by the hypothesized

model. Additionally in the X-ray model, V54 and S115 would be expected to have moderate collisions with DOGS-NTA-Ni. Figure 3-7 shows the X-ray and EPR orientations of GM2AP on lipid bilayers to distinguish the original model from the one determined from these power saturation studies. Again, spheres represent sites mutated to CYS for EPR measurements and the color code indicates the relaxation values of $\Pi^{\text{DOGS-NTA-Ni}}$ (low collisions = blue and high collisions = red). It is clear from this Figure 3-7 that T90R1 in the original model would be inaccessible to DOGS-NTA-Ni, as it is positioned far from the bilayer surface.

Discussion

In addition to functioning as an accessory protein in ganglioside breakdown, it has been shown, *in vitro,* that GM2AP can transfer phospholipids (*41*) and fluorescent lipids (*36*) between vesicles, can bind and consequently inhibit platelet activating factor (PAF) (*33, 42*), as well as participate in presenting lipid antigens to T cells (*79*). Each of these functions involves binding and extracting lipids from bilayers, but the mechanistic details of lipid extraction are not known. Determining the membrane bound orientation of GM2AP on lipid vesicles may provide insights to these details.

Power saturation EPR spectroscopy has been used as a structural biology tool for determining surface-bound orientations of numerous membrane binding proteins including human group IIA phospholipase A_2 (*72*) and C2 domains (*53, 67*). This methodology has advanced from measuring the depth of spin labeled proteins in bilayers to providing intricate details of Euler angle rotations of the membrane docked protein. Here, we do not report a high-resolution orientation of GM2AP on POPC bilayers, but our collisional data with DOGS-NTA-Ni does provide evidence that the protein is rotated such that the face of the hydrophobic pocket interacts with the bilayer. This orientation differs from the model proposed from analysis of the

X-ray structures (*30, 31, 77*), which postulated that the apolar loop (Fig 3-2, Fig 3-8) might penetrate into the bilayer.

Figure 3-7 compares the orientation of GM2AP binding to lipid bilayers obtained from analysis of X-ray structures with the model that is more consistent with our EPR results. Sites of high and low collision with DOGS-NTA-Ni are highlighted in red and blue, respectively. Rotating the protein such that the high collision sites are nearest the bilayer and low collision sites are not in proximity for collisions with DOGS-NTA-Ni positions the residues lining the entire hydrophobic pocket on the bilayer surface. This orientation is plausible because it is known that lipids occupy the hydrophobic cavity, so its opening must face the bilayer in order for the lipids to enter the binding pocket. One side of the cavity entrance consists of a highly flexible region called the "mobile loop" and spans residues V122 to L132. This region of the protein was seen in two conformations in X-ray structures, where one conformation, presumably the "open" conformation, widens the opening to the cavity while the other conformation of the loop is tucked into the pocket and "closes" the entrance. We could propose from the surface-bound orientation and the dynamic nature of this stretch of amino acids that positioning the entire face of hydrophobic pocket creates a favorable environment for the phospholipid acyl tails to flip from the bilayer into the hydrophobic pocket of membrane-bound GM2AP and that the opening and closing of the mobile loop could aid in facilitating lipid extraction. We can compare our model of GM2AP lipid binding to information known about other lipid transfer proteins. Sec14p is a phosphatidylinositol transfer protein and has a hydrophobic phospholipid binding pocket that is thought to be gated by an α-helix. EPR studies by Smirnova, *et al.* provided many important details to phospholipid binding (*73*). First, the orientation of the spin labeled phospholipid positions the acyl tails within the cavity and the lipid headgroup points out toward

solution. The flexibility of the acyl tails increased as distance from the headgroup increased down the *sn*-2 acyl chain, suggesting tighter binding at the headgroup region. These studies also revealed that Sec14p creates a polarity gradient that accommodates binding phospholipids, such that the interior of the protein, the part occupied by the ends of the acyl tails, is aprotic and gradually changes to a more protic environment around the lipid headgroup. This gradient was postulated to be the driving force of lipid extraction. Like Sec14p, GM2AP binds GM2 such that the acyl tails of the ceramide moiety of GM2 occupy the hydrophobic pocket and the oligosaccharide headgroup is solvent accessible. Both of these proteins also share the feature of having a relatively spacious lipid binding pocket, as was demonstrated by mobility parameters of DOXYL-labeled lipids bound to Sec14p (*73*) and by measuring the dimensions of the hydrophobic cavity determined by analysis of the X-ray structure of GM2AP (*31*). Although GM2AP has a larger binding pocket than Sec14p, the spaciousness of these pockets supports that these proteins can bind a variety of nonspecific lipids and carry out multiple functions.

The orientation of GM2AP on the bilayer surface shown in Figure 3-7 is further supported by inspecting the specific residues that surround the cavity. A number of hydrophobic amino acids (valine, phenylalanine, and leucine), small polar amino acids (serine and threonine) as well as three aspartic acid and seven glutamic acid residues line the binding pocket. Figure 3-8 highlights the acidic residues in red. The presence of hydrophobic residues is expected given that the protein interacts with lipid bilayers. It is interesting; however, that a number of aspartic acid and glutamic acid residues are also found in this region of GM2AP. At pH < 5, it is likely that the majority of these sites are protonated. Protonation of aspartates and glutamates would lower the Born repulsion energy needed to insert into the lower dielectric medium of the bilayer. Protonated aspartates and glutamates are still polar, so deep penetration into the bilayer is not

expected, but rather these side chains would be expected to associate with the phosphate-glycerol head group region of the lipid bilayer. If we consider that the collision data with DOGS-NTA-Ni show that GM2AP binds to bilayers at pH 4.5 and not at pH 8, it is apparent that these acidic residues act as a "pH switch" that modulates GM2AP binding to bilayers simply as a result of the charge state of the acidic amino acid side chains. We believe these residues play a crucial role in driving binding to lipid bilayers at acidic pH.

Traditional power saturation experiments that use oxygen and NiEDDA colliders has provided a means for measuring protein orientations on and within lipid bilayers, and has typically been used for either integral membrane proteins or for membrane proteins that remain bound to bilayers. This is the first report of using power saturation to study a protein that undergoes exchange on and off the bilayer surface. Incorporating a surface-bound paramagnetic collider through use of DOGS-NTA-Ni has allowed us to effectively take a snapshot of only those proteins bound to the bilayer. This strategy allows for the mapping of these regions of the protein that were accessible to collisions with DOGS-NTA-Ni, and leads to a low resolution orientation of GM2AP on POPC bilayers, which was not attainable by the traditional method. Being able to measure collisions of spin labels with surface-bound reagents is significant in that the power saturation methodology has now been extended to studying proteins in exchange on lipid bilayers.

In summary, site directed spin labeling and power saturation EPR were used for determining a bilayer bound orientation of GM2AP on POPC vesicles. This work also shows how spin labels at certain sites on GM2AP loops can interfere with non-specific lipid extraction through steric effects. Performing power saturation with the surface bound metal collider, DOGS-NTA-Ni, provides a means for mapping those sites of a protein in contact with the bilayer

surface for proteins in equilibrium between surface-bound and in-solution states. The model supported by our EPR data is different from the previously proposed model (*30, 63*) based upon X-ray diffraction data (*31, 33, 77*), and has a similar orientation to that proposed for Sec14p (*73, 74*).

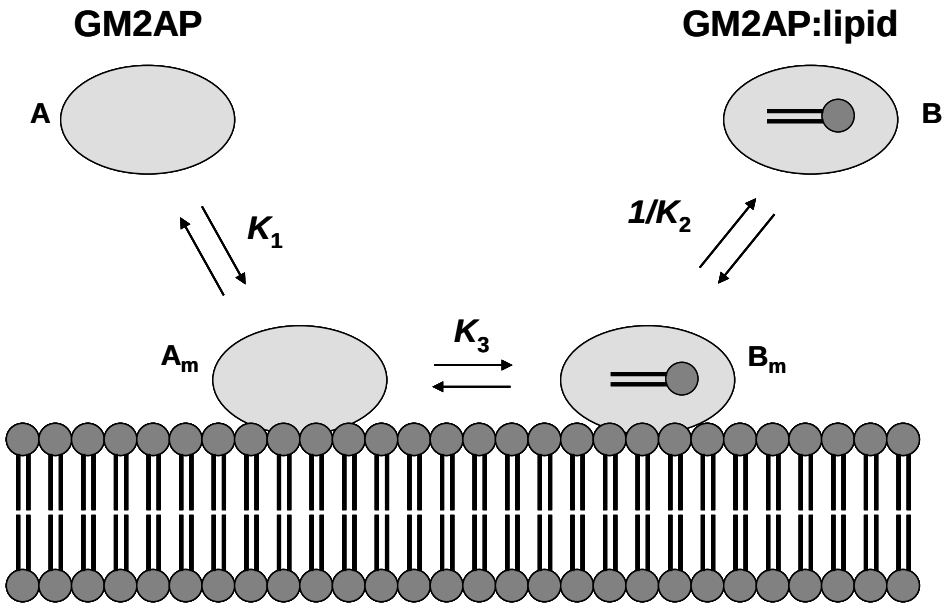

Figure 3-1. Cartoon showing how GM2AP interacts with lipid vesicles. An equilibrium is established with apo protein (A) in solution or associated with the bilayer surface (A_m), or as a protein:lipid complex that is bound (B_m) to lipid bilayers or in solution (B).

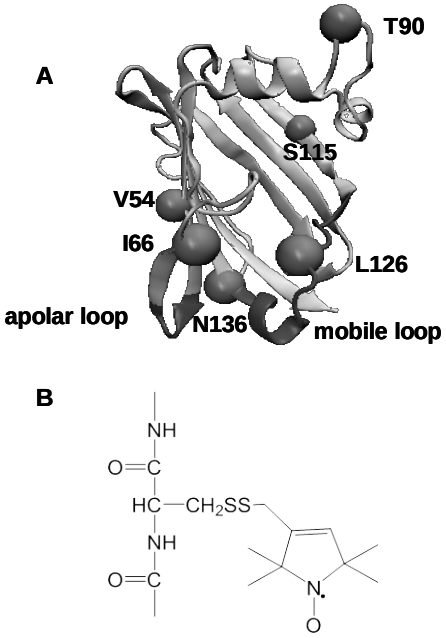

Figure 3-2. X-ray structure of GM2AP and site directed spin labeling scheme. (A) Ribbon diagram of GM2AP (PDB 1G13) with sites mutated to cysteine residues for spin labeling with methanethiosulfonate shown by beads at the Cα position, the apolar and mobile putative membrane binding loops highlighted in dark grey. (B) Scheme for attaching the MTSL spin label to mutant cysteine residues via disulfide bond formation producing a modified side chain referred to as R1.

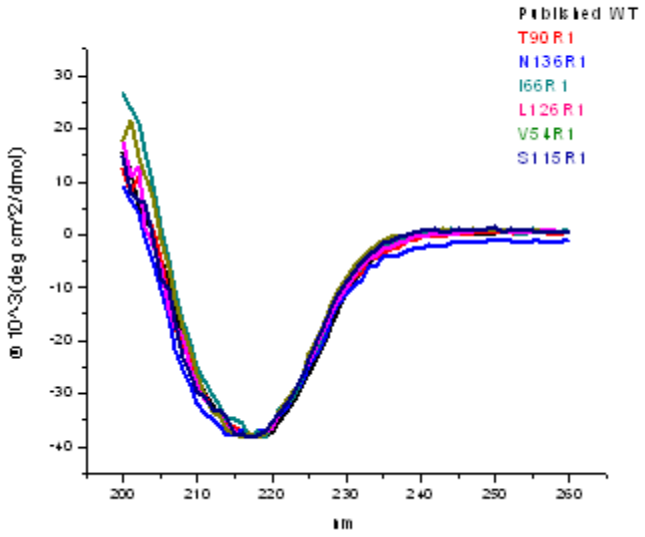

Figure 3-3. Overlay of circular dichroism spectra of 20 µM GM2AP WT and spin labeled constructs in 100 mM NaCl, 50 mM phosphate buffer, 2.5% glycerol, pH 7.0. The spectra were recorded using a 1 mm light path cuvette at 25 ºC.

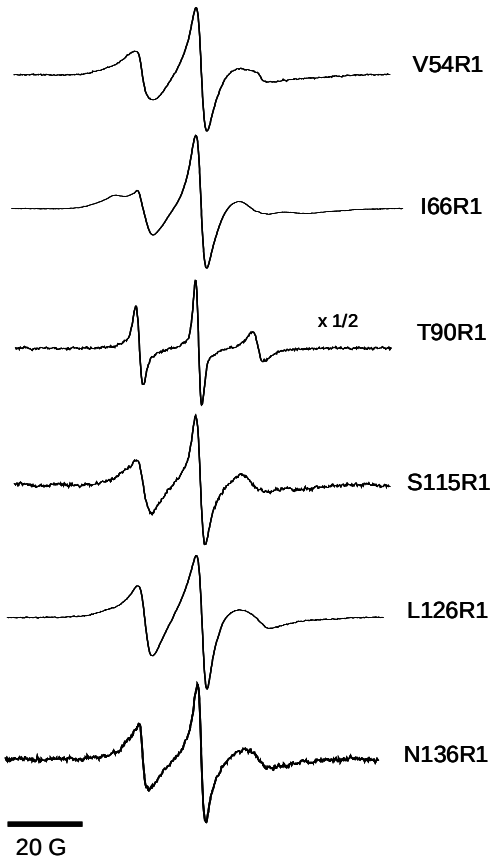

Figure 3-4. Double integral area normalized 100 G EPR spectra of the GM2AP R1 labeled CYS constructs. The X-band continuous wave EPR spectra were collected in 50 mM Tris buffer, pH 8.0 at ambient temperature and area-normalized.

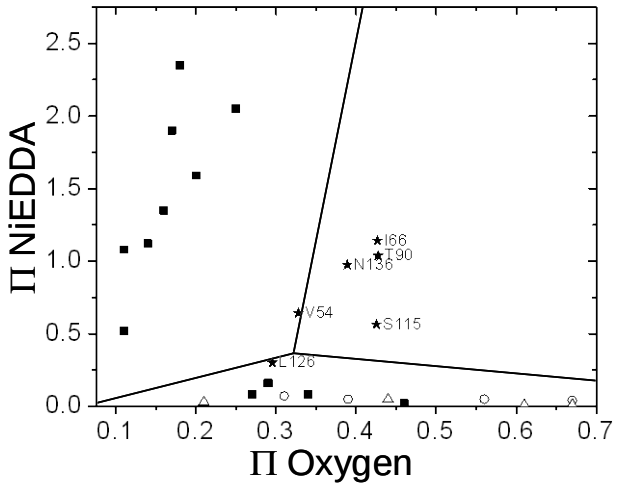

Figure 3-5. Plot of collision parameters, Π, for spin labeled sites of GM2AP, C2 domain of cPLA2, bacteriorhodophsin, and doxyl-labeled lipids. Points on the graph are Π values for GM2AP at pH 4.5 (solid stars), of C2 domain of cPLA2 bound to PC/PS bilayers (3:1) (solid squares), of bacteriorhodopsin (open triangles) and of doxyl-labeled lipids (open circles) (*61*). Plotting Π^{NiEDDA} versus Π^{Oxygen} has been used to differentiate aqueous exposed sites from sites buried within the lipid bilayer based on where the points cluster on the graph. The aqueous exposed sites occupy the upper left region of the plot and the lipid exposed sites fall in the lower region along the x-axis. All but two spin labeled sites of GM2AP gave collision data that places them outside the defined regions of the Π^{NiEDDA} versus Π^{Oxygen} plot.

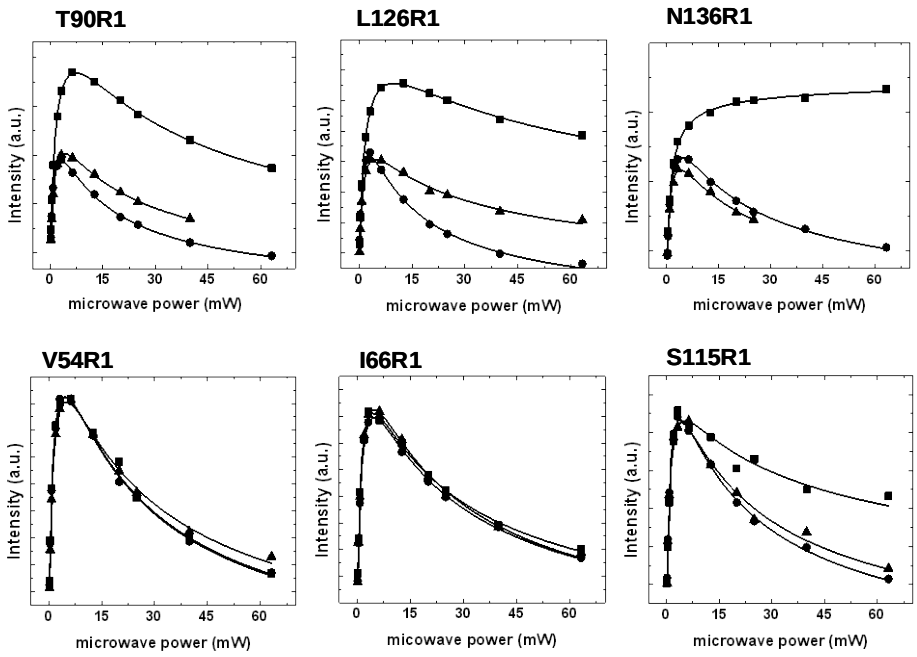

Figure 3-6. Power saturation curves for GM2AP R1 constructs. GM2AP R1 constructs were mixed with POPC:DOGS-Ni-NTA(9:1) LUVs under three different experimental conditions: pH 8 (▲), pH 4.5 (■), and pH 4.5 + EDTA (●).

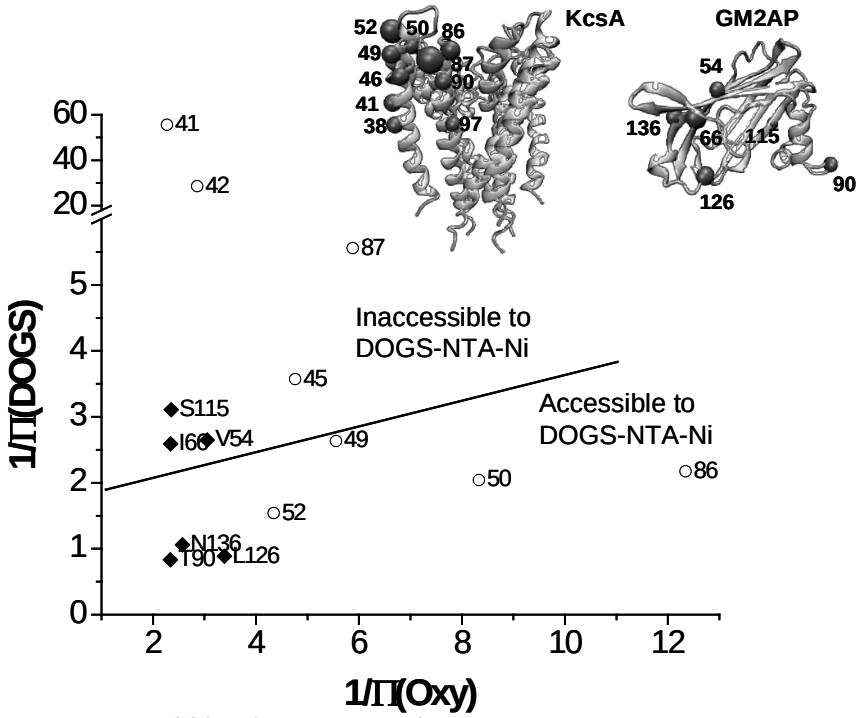

Figure 3-7. Inverse plot of $\Pi^{\text{DOGS-NTA-Ni}}$ versus Π^{Oxy} for spin labeled GM2AP sites shown as solid diamonds and KcsA sites shown as open circles. Crystal structures of both GM2AP (PDB = 1G13) and KcsA (PDB = 1BL8) with the Cα positions of sites of spin label attachment are shown as spheres. Collision values for KcsA with DOGS-NTA-Ni were taken from (*66*), and oxygen collision parameters were taken from (*71*). The line provides a general separation of data points that were found to be accessible and inaccessible to DOGS-NTA-Ni. Differences in values found for sites of GM2AP that were inaccessible to DOGS-NTA-Ni compared to inaccessible sites of KcsA arise from differences in oxygen collisions. Spin labeled sites of KcsA that were inaccessible to DOGS-NTA-Ni were located on the transmembrane helices that were within the bilayer, and therefore, had larger oxygen collision values. GM2AP is surface associated to lipid bilayers, and spin labeled sites of GM2AP that were inaccessible to DOGS-NTA-Ni were not in the bilayer, as seen for KcsA. The inaccessible sites of GM2AP were located in the aqueous phase rather than the bilayer, which resulted in lower oxygen collisions compared to KcsA.

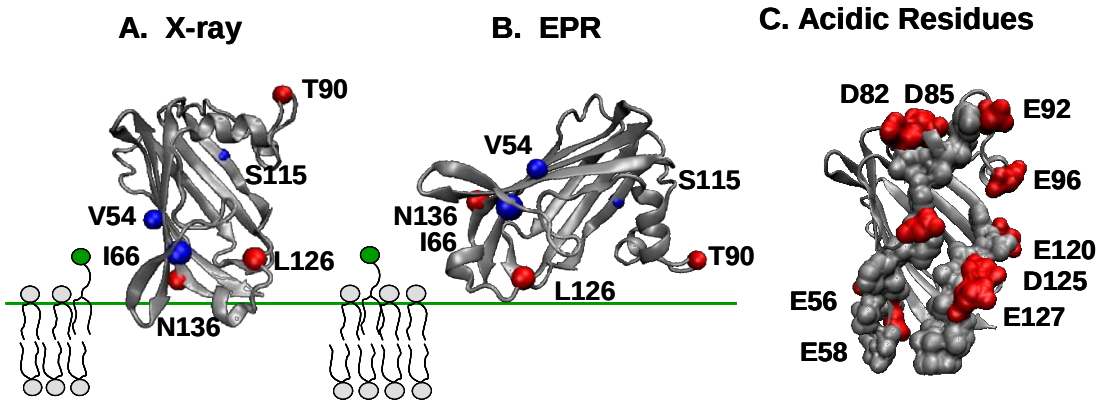

Figure 3-8. Comparison of membrane bound orientations of GM2AP from crystal structure analysis and power saturation experiments, and highlighting of acidic residues. A) Model of the membrane bound orientation of GM2AP proposed from X-ray structure analysis (*31*) and, B) the orientation of GM2AP on POPC bilayers after power saturation experiments, showing sites of high collisions (red) and low collisions (blue) to DOGS-NTA-Ni. The DOGS-NTA-Ni lipid is represented by the cartoon lipid containing the green sphere. C) Ribbon diagram of GM2AP with the acidic residues shown as space filling form in red and nonpolar residues in grey. These acidic residues that surround the hydrophobic cup may act as a "pH switch" for GM2AP binding to bilayers.

Table 3-1. Half-life values for dansyl extraction from POPC LUVsa and collision values for GM2AP WT and R1 spin labeled constructs

Mutant	$t_{1/2}$ (minutes)	Π^{oxy}	Π^{NiEDDA}	Π^{DOGS}	$\Pi^{DOGS + EDTA}$
WT	1.5 ± 0.1	--	--	--	--
V54R1	0.9 ± 0.1	0.14 ± 0.06	0.52 ± 0.07	0.09 ± 0.05	0.10 ± 0.04
I66R1	NA	0.43 ± 0.07	1.14 ± 0.08	0.07 ± 0.05	0.09 ± 0.04
T90R1	1.8 ± 0.2	0.42 ± 0.07	1.04 ± 0.10	0.48 ± 0.05	0.10 ± 0.03
S115R1	5.2 ± 0.8	0.40 ± 0.12	0.57 ± 0.15	0.08 ± 0.11	0.06 ± 0.05
L126R1	1.7 ± 0.1	0.30 ± 0.04	0.30 ± 0.12	0.44 ± 0.06	0.01 ± 0.04
N136R1	1.6 ± 0.3	0.39 ± 0.07	0.97 ± 0.08	0.37 ± 0.10	0.20 ± 0.06

a Dansyl extraction assays were performed at pH 4.8 with 5 μM final protein concentration and 1 μM final lipid concentration at 20°C.

Table 3-2. $P_{1/2}$ values for DOGS-NTA-Ni extraction experiment with L126R1.

Experiment Number	$P_{1/2}$ value of L126R1 + vesicles	$P_{1/2}$ value of L126R1 supernatant	$P_{1/2}$ value of L126R1 supernatant + EDTA
1	5.33 ± 0.11	3.19 ± 0.11	2.83 ± 0.10
2	4.66 ± 0.07	3.16 ± 0.15	2.56 ± 0.06
Average	5.00 ± 0.09	3.18 ± 0.13	2.70 ± 0.08

CHAPTER 4
CONFORMATIONAL HETEROGENEITY OF THE MOBILE LOOPS

Introduction

As was previously discussed, the GM2 activator protein (GM2AP) functions as a lipid binding protein by solublizing ganglioside GM2 from intralysosomal vesicles to form a protein:lipid complex in solution. The ability of GM2AP to bind and transfer nonspecific lipids, such as the fluorescently labeled octadecylrhodamine (R-18) lipid and the dansyl-labeled phosphatidylethanolamine (DDHPE), was also described. Chapter 3 discussed the use of site directed spin labeling in conjunction with power saturation electron paramagnetic resonance spectroscopy (EPR) to determine the membrane bound orientation of GM2AP on phosphatidylcholine lipid bilayers. Chapter 4 now takes a look at two flexible loops in GM2AP that are potentially involved in the lipid binding event.

The X-ray structure of GM2AP has been solved previously (*31*) and reveals that GM2AP is structurally unique compared to the other saposins. Chapter 1 described the structural homology of saposins A-D, where they all have the characteristic "saposin fold" that consisted of four or five α-helices that are held together by three disulfide bonds. GM2AP, however, consists of eight β-strands that fold into a β-cup topology and contains four structural disulfide bonds (*31*). As the name suggests, the shape of the β-cup topology is similar to that of a cup, where the interior of the "cup" is lined with hydrophobic residues, making it a suitable cavity for interacting with lipids. The volume of the hydrophobic cavity is roughly six times larger than the volume of a ceramide moiety (500 $Å^3$). Several loop regions that line the entrance to the lipid binding cavity of the protein were identified as having structural flexibility due to large positional differences and high *B* factors (*31*). In fact, three different conformations of GM2AP were seen in the crystal structure and were identified as chains A, B, and C (Fig 4-1). These

regions of high flexibility (highlighted in red in Fig 4-1) are of particular interest because protein mobility is often related to its function. One of these flexible loop segments, referred to as the "apolar loop," spans residues 58 to 78, and subtle differences are seen when comparing the three chains. Chains A and B of GM2AP have very similar conformations of the "mobile loop" region, spanning residues 121-132, where the loop is such that the side chains of the amino acid residues are pointing out towards the aqueous medium, which widens the entrance to the lipid binding cavity. The position of this loop in chains A and B are thought to be an "open" conformation of GM2AP. In chain C, the residues towards the end of the mobile loop, Ser130 to Thr133, are flipped so that their side chains point in towards the interior of the hydrophobic pocket. This conformation of the mobile loop amino acids in chain C significantly narrows the entrance to the cavity. Thus, the two positions of the mobile loop are likely to be related to the function of GM2AP through controlling the diameter of the entrance to the lipid binding cavity and providing a channel for directing the lipid into the cavity (*31*).

The X-ray structure for GM2AP with a bound phospholipid as well as a structure of GM2AP crystals grown in the presence of GM2 has also been reported (*77*). These data suggest that GM2AP has different modes for binding specific and nonspecific ligands. Electron density for nonspecific phospholipids, such as phosphatidylglycerol, for example, was found towards the center of the hydrophobic cavity and widened deep inside the pocket. These data suggest that the lipid is bound in an orientation that positions the polar head group near the apolar and mobile loop regions and the acyl tails extend into the pocket, with their methyl termini in proximity to the short α-helix. Crystals grown in the presence of GM2, the specific ligand of GM2AP, showed electron density in a different region of the lipid binding pocket and was assumed to represent the acyl chains of the ceramide backbone of GM2. The density interpreted to be the acyl tails

was positioned against one side of the lipid binding cavity, with the ends of the tails occupying the same space deep in the cavity as the acyl tails of the bound phospholipid, but at roughly a 45° angle compared to the phospholipid tails. The tetrasaccharide of GM2 was not resolved, suggesting that lipid head group is not ordered, but according to the placement of the ceramide tail, the oligosaccharide group would extend into solution near the α-helix. This binding mode for GM2 is plausible because the hydrophobic nature of the binding cavity would not accommodate a hydrophilic oligosaccharide group and because the short α-helix is the region of GM2AP that associates with Hex A for removal of the terminal GalNAc group of GM2 (*32*).

X-ray crystallography is a power method for learning about positions of atoms and the overall structure of proteins, however, the technique often requires that the proteins be subjected to unnatural conditions in order for crystal formation to occur. The question arises, "are features of the protein that are seen in the crystal structure are actually present in solution?" For the case of GM2AP, do the multiple conformations in the crystal structure, which change the diameter of the entrance to the lipid binding cavity, reflect a conformational change upon lipid binding? It is possible that the "open" conformation of the mobile loop seen in chains A and B could be the conformation in the absence of lipid, and upon lipid binding, GM2AP undergoes a conformational change to the "closed" conformation seen in chain C to stabilize the bound lipid. To answer this question, the system must be studied spectroscopically.

Site directed spin labeling (SDSL) with electron paramagnetic resonance spectroscopy (EPR) is a powerful spectroscopic tool for studying protein dynamics and conformational changes (*49, 56, 80*). This technique has been used to study proteins that undergo order-to-disorder transitions (*81*), and is therefore a well-suited method probing the local dynamics of the loops in solution because EPR line shapes reflect local motion of the protein. If, in the absence of

lipid, the mobile loop is in a dynamic, open conformation and then changes to a (presumably) more ordered, closed conformation upon lipid binding, the change in mobility of the spin label in the loop will be detected in the EPR lineshape. Ten sites were chosen for single cysteine mutation and spin labeling (Fig 4-2). EPR spectra for the ten single mutants were recorded in solution and with GM2 micelles, and the solution EPR spectra were simulated using the microscopic order macroscopic disorder model (MOMD) of Freed and colleagues (*82*). Spin labeled sites in the apolar and mobile loops had line shapes that required a two component fit, where the two components corresponded to mobile and immobile components of the EPR spectra. Sites on the back of β-strands, the solvent accessible surface of the α-helix, and in an unstructured loop all produce line shapes with a single component fit. Finally, two sites were chosen, one on the apolar loop and one on the mobile loop, for variable temperature EPR experiments to obtain thermodynamic information about loop motion. Results from these experiments suggest that the mobile loop is simply dynamic and undergoes exchange between the two conformations seen in the X-ray structure and that the two conformations are not a result of lipid binding.

Materials and Methods

Protein Purification

Cysteine mutants of the GM2 activator protein were expressed in *E. coli*, purified and spin labeled as described in Chapter 3. Cysteine mutants were allowed to react with the MTSL to form the modified side chain R1 (Fig 2-3).

Circular Dichroism Spectroscopy

CD spectra were measured with an Aviv-400 Spectropolarimeter at 25ºC using a 1 mm path length cuvette. Data were collected from 260 nm to 190 nm every 1 nm with a 1 nm bandwidth**.** Each sample was measured twice and the two scans were averaged. CD spectra of

WT and cysteine mutant constructs of GM2AP were measured for protein concentrations ranging from 50 μM to 80 μM in 50 mM phosphate, 150 mM NaCl, 2.5% glycerol pH 7.0 buffer.

CW-EPR Measurements

Continuous wave EPR spectra were collected on a modified Bruker ER200 spectrometer with an ER023M signal channel, an ER032M field control unit and equipped with a loop gap resonator (Medical Advances, Milwaulkee, WI). Solution spectra of GM2AP mutants were recorded with protein samples in sealed round capillaries, 0.60 mm x 0.84 mm x 100 mm (Fiber Optics Center, Inc.; New Bedford, MA), at room temperature and with 3.16 mW incident power. Concentrations of protein ranged from 100-200 μM in either 50 mM Tris pH 8.0 or 50 mM NH_4Ac pH 4.5 buffers. All EPR spectra were recorded with an incident microwave power of 3.16 mW and appropriate modulation amplitude at 100 kHz that did not distort the EPR spectrum. Labview software was used for baseline correction, free spin subtraction (when applicable) and double integral area normalization, and was generously provided by Drs. Christian Altenbach and Wayne Hubbell (UCLA). Spectra were recorded for each of the GM2AP cysteine mutants in solution (50 mM Tris HCl pH 8.0) and mixed with GM2 micelles (50 mM ammonium acetate pH 5.0).

Variable Temperature Experiments

Continuous wave X-band EPR spectra were recorded for aqueous (50 mM Tris HCl pH 8.0 buffer) GM2AP spin labeled constructs at temperatures ranging from 6 °C to 35 °C in 5 °C increments, where the sample was allowed to equilibrate at each temperature for at least 20 minutes. The temperature was controlled by positioning a glass dewar (Wilmad-Labglass, Buena, NJ) around the protein sample and loop gap resonator connected to a nitrogen gas flow that

passed through a copper coil submerged in a waterbath (Thermo Scientific Neslab RTE-7 digital one (– 25°C to 150°C ± 0.01°C) of 40% ethylene glycol in water.

Simulation of EPR Line Shapes

Electron paramagnetic resonance (EPR) spectra of R1 constructs were simulated using the microscopic order macroscopic disorder (MOMD) model of Freed and colleagues that uses nonlinear least squares analysis (*82, 83*). In the MOMD model, three coordinate frames are used to describe nitroxide motion: the magnetic tensor frame (x_M, y_M, z_M), the rotational diffusion tensor frame (x_R, y_R, z_R), and the director frame. It is customary in the molecule-fixed magnetic tensor frame to draw the N – O bond of the nitroxide along the x_M axis and the nitroxide *p*-orbital along the z_M axis (Fig 4-2). This magnetic frame is the principle frame for the nitroxide hyperfine (**A**) and **g** tensors. The second coordinate frame is the principle frame of the rotational diffusion tensor. The magnetic frames and the rotational diffusion frames are not coincident, and their relationship is defined by the Euler angles required to rotate the diffusion frame into the magnetic frame. These Euler angles are the diffusion tilt angles α_D, β_D, and γ_D. Simulations of experimental EPR line shapes are strongly dependent on β_D, the angle between the *z*-axis of the rotational diffusion frame and the *z*-axis of the magnetic frame (Fig 4-2), but only weakly dependent on α_D and γ_D (not shown in Fig 4-3). The MOMD model simulates anisotropic motions by applying an ordering potential (*U*) to constrain the motion of z_R. Because methanethiosulfonate (MTSL) spin labels were attached to GM2AP at solvent exposed sites, the following expression can be used to calculate the ordering potential to describe the motion of nitroxides (*83*).

$$U(\theta) = -\frac{1}{2} k_b T C_{20} (3\cos^2\theta - 1) \qquad (4\text{-}1)$$

In this equation, C_{20} is a coefficient for the ordering potential, and θ is the instantaneous angle between z_R and the symmetry axis of the ordering potential (*49, 82, 83*). Finally, the third coordinate frame is the director frame, and its *z*-axis is defined by the axial symmetry of the ordering potential. This director frame is fixed to the protein backbone at the residue of interest for describing covalently attached nitroxides under an ordering potential. Anisotropic motion arises from the existence of a restoring potential and can be characterized by an order parameter, S_{20}.

$$S_{20} = \frac{1}{2}\left\langle (3\cos^2\theta - 1) \right\rangle \tag{4-2}$$

An individual protein forms an angle, ψ, between z_D and the external magnetic field. A sample contains infinite orientations of proteins and, therefore, the final spectrum is summed over all ψ (*83*).

Results

Ten single cysteine mutants were expressed and purified from *E. coli*, and spin labeled with MTSL (where the modified side chain is denoted as R1) to generate the following spin labeled constructs: V54R1, A60R1, I66R1, I72R1, L87R1, T90R1, S115R1, L126R1, S130R1, and N136R1 (Fig 4-2). Six of these spin labeled sites are located in the apolar (A60R1, I66R1, I72R1) and mobile loop (L126R1, S130R1, and N136R1) regions of GM2AP and were selected to investigate the mobility of the loops in the absence and presence of GM2 ligand using EPR spectroscopy. Simulation of these line shapes resulted in a two component fit. The remaining four sites were selected as potential sites for having line shapes that require only one component to obtain the best fit and will be discussed later in the chapter.

EPR spectral line shapes for the six R1 labeled GM2AP constructs in solution (50 mM Tris HCl pH 8.0) and with GM2 micelles (50 mM ammonium acetate pH 5.0) are overlain in Figure

4-4. A60R1, L126R1, and N136R1 have line shapes consistent with fairly mobile and solvent accessible sites on proteins (*49*). Sites I66R1, I72R1 and S130R1 have broadened EPR spectra with fine structure seen in the low field resonances and indicate that these spin labeled sites are more structured regions of GM2AP. Although not the broadest line shape, I72R1 does have a broadened spectrum with more noise than the others, and could be a result of attaching a spin label three residues away from a native cysteine that participates in a disulfide bond. Overall, no significant change in each of the line shapes is seen upon addition of GM2 micelles. Small changes in intensity for line shapes of A60R1, I 72R1 and N136R1 are seen, but could be a result of changes in temperature between measurements. Figure 4-4 also shows circular dichroism spectra (CD) for wild type GM2AP at pH 4.5 and 7.0, and at pH 4.5 with and without GM2 micelles, and no change in secondary structure is seen under these conditions.

Solution EPR line shapes for the ten spin labeled GM2AP constructs were simulated using the microscopic order macroscopic disorder model (MOMD). Four sites, V54R1, L87R1, T90R1, and S115R1 were simulated using a single component fit, and the overlay of the experimental and simulated spectra are shown in Figure 4-5. The six sites located in the apolar and mobile loops required two components in the fit. The two components correspond to a mobile and immobile component. This result was interesting because it corresponds to flexible regions identified in analysis of the X-ray structure. The overlay of the experimental and simulated lineshapes, as well as an overlay and corresponding percentages of the mobile and immobile components are also shown in Figure 4-5.

One question that was critical to address was whether the two components were due to protein dynamics or if it was a result of having misfolded GM2AP present in the sample. Recall that GM2AP has eight native cysteines that form four structural disulfide bonds that are required

for proper folding and function. Overexpression of GM2AP in the reducing environment of *E. coli* results in the protein forming inclusion bodies, because an oxidizing environment is favorable for disulfide bond formation. The purification of GM2AP from *E. coli* requires isolation and denaturation of the inclusion bodies, followed by a refolding step. During refolding, the four disulfide bonds of recombinant GM2AP must form correctly. Several steps were taken to ensure that the protein used in EPR experiments is homogeneous (Fig 4-6). The final step of protein purification is gel filtration chromatography using an S-200 column that separates properly folded protein (elution volume 65 mL, corresponding to an 18 kDa protein) from misfolded or aggregated GM2AP, which eludes at a higher molecular weight (35 mL elution volume). A representative chromatogram showing two elution peaks is shown in Figure 4-6. Fractions from both peaks were analyzed by circular dichroism and EPR spectroscopy. The CD spectrum of 65 mL elution fractions matched published WT spectra while the 35 mL fractions diverged from WT spectra at lower wavelengths (Fig 4-6). EPR spectra were also collected for samples from both elution peaks. Differences between the two samples can be seen in the low field peak (Fig 4-6).

Since we are confident that the EPR samples are homogeneous samples, we wanted to further investigate the two component sites to see if these results relate to the protein structure. Variable temperature EPR has been used to study the conformational change of a transmembrane sequence of the transducer domain of *N. pharaonis* halobacterial transducer of rhodopsins II (NpHtrII) in lipid membranes (*84*). Sites L126R1 on the mobile loop, and I66R1 on the apolar loop, were selected for the variable temperature EPR experiments. If these regions of the protein are in conformational exchange, the equilibrium of the two populations should be changed with temperature. Solution EPR spectra were collected for each spin labeled sample (50 mM Tris HCl

pH 7.0) at temperatures ranging from 7° to 30° C. Samples equilibrated for at least 20 minutes at each temperature prior to collection of spectra (Fig 4-7). The EPR line shapes were then simulated using the MOMD model to extract correlation times and fractions of populations of the two components (Fig 4-7). The percentage of the mobile and immobile components obtained from the line shape fits for L126R1 and I66R1 were plotted as a function of temperature (Fig 4-8). The data for L126R1 show a temperature dependent change in the percentages of mobile and immobile components. At low temperatures, the percent mobile and immobile components are about 10 and 90, respectively. With increasing temperature, the percent mobile component increases and the percent immobile decreases until almost equal populations of the two components are seen at 25° C. The spectra for I66R1, however, did not show a temperature dependent change in the percentage of the two components.

Because the EPR line shapes for L126R1 showed a temperature dependent change in mobile and immobile components, the natural logarithm of the ratio of the fractions of the two components were plotted as a function of inverse temperature in order to obtain an activation energy of loop motion (Fig 4-8). The data for I66R1 show no temperature dependent correlations; however, data for L126R1 do show a linear dependence, and the activation energy calculated from the slope of the line (-8.0 ± 0.5) was found to be about 16 cal/mol. Such a low activation energy therefore suggests that the mobile loop of GM2AP is able to undergo exchange between the two conformations seen in the X-ray structure at room temperature.

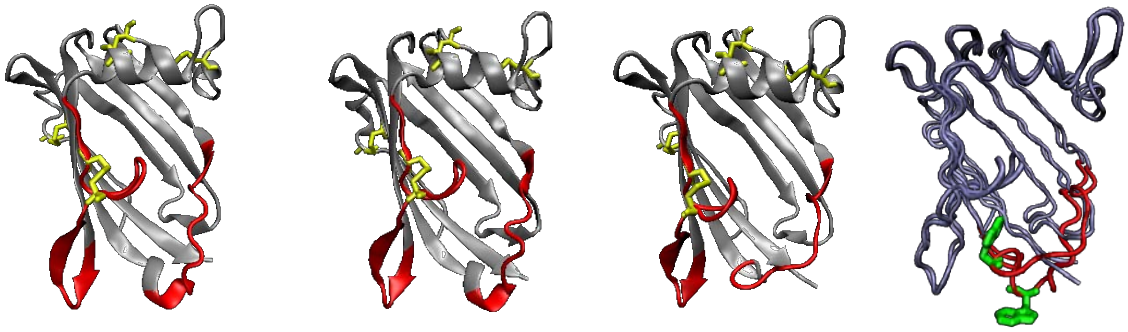

Figure 4-1. X-ray structure ribbon diagrams of the three conformations of GM2AP seen and the overlay of chains A and C. For chains A-C, the four disulfide bonds are shown as sticks in yellow, and the mobile loops that span residues 58 to 78 and 121 to 132 is highlighted in red. The overlay highlights Trp131 to emphasize the rotation of the side chains in the two conformations.

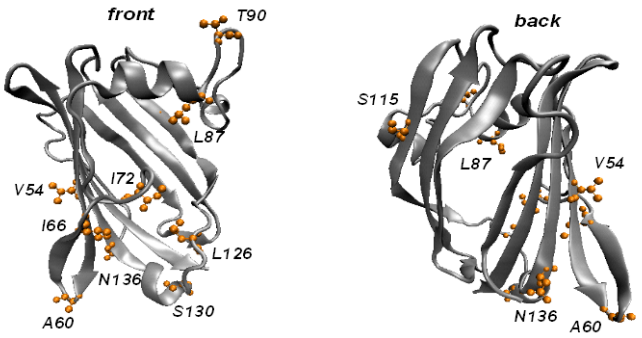

Figure 4-2. Ribbon diagram of GM2AP with single cysteine mutation sites shown in CPK style.

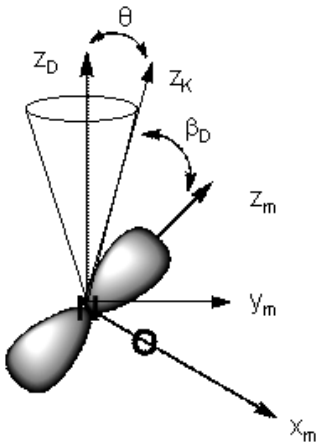

Figure 4-3. Coordinate frames used in the MOMD model to describe nitroxide motion.

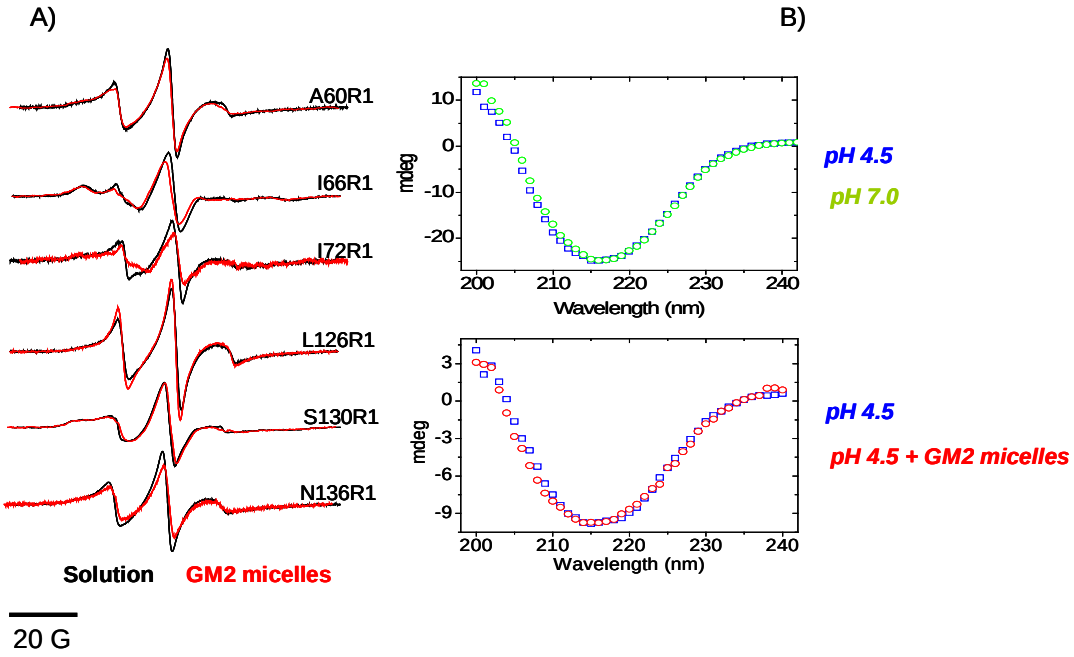

Figure 4-4. EPR spectra of spin labeled GM2AP constructs in the absence and presence of GM2 ligand and corresponding circular dichroism (CD) spectra of GM2AP as a function of pH and ligand. A) Continuous wave X-band EPR spectra of spin labeled GM2AP CYS mutants in solution (black) and with GM2 micelles (red) are overlaid. No significant changes in the EPR line shapes are seen upon ligand addition. B) CD spectra of WT GM2AP at pH 7.0 (green) and pH 4.5 (blue), and in the absence (blue) and presence (red) of GM2 micelles. Again, no change in the overall secondary structure of GM2AP was detected.

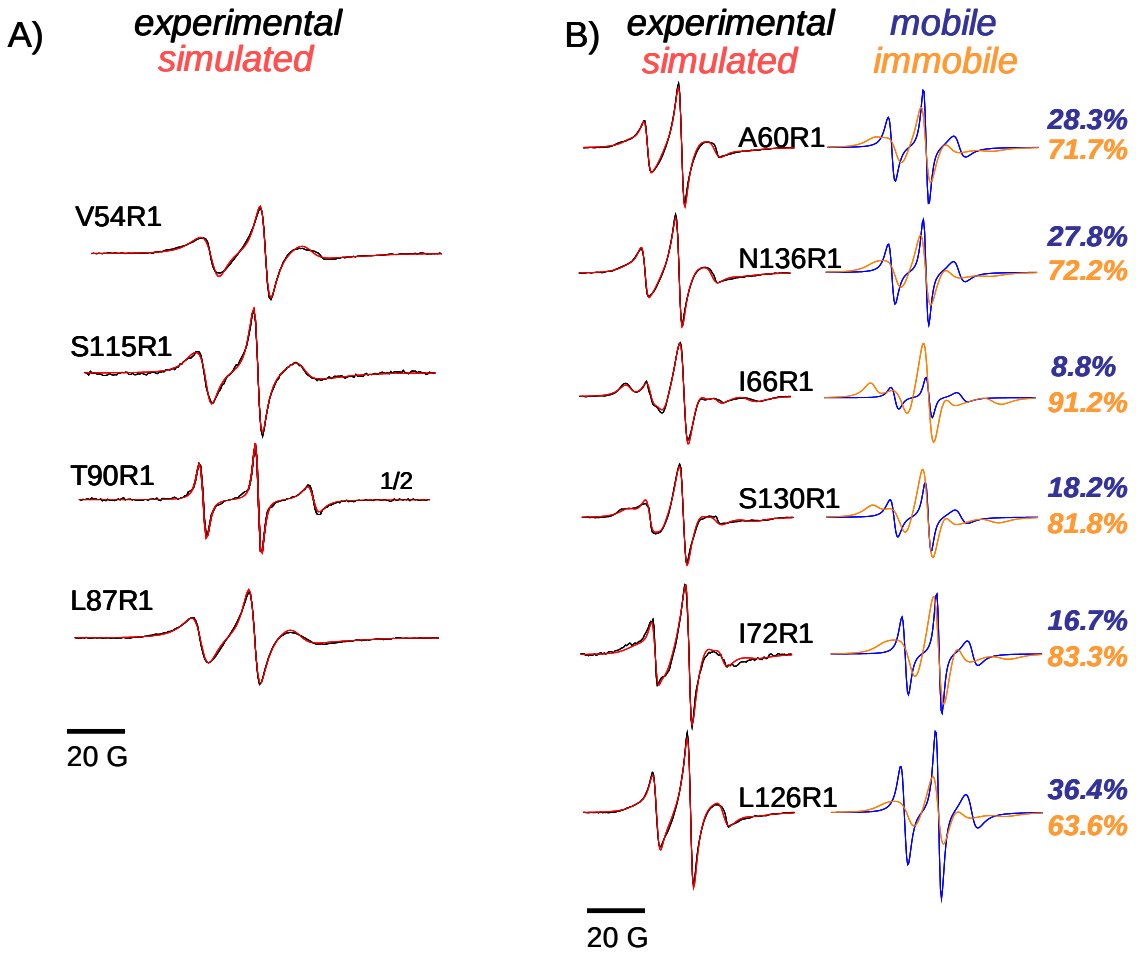

Figure 4-5. Experimental and simulated X-band EPR spectra for single cysteine mutant constructs. A) Overlay of experimental (black) and simulated (red) continuous wave X-band EPR spectra for sites that have a single component fit. B) Experimental (black) and simulated (red) EPR spectra for spin labeled sites with two component fits. The mobile (blue) and immobile (orange) components of the simulated fit and the corresponding percentages of each component are shown for each.

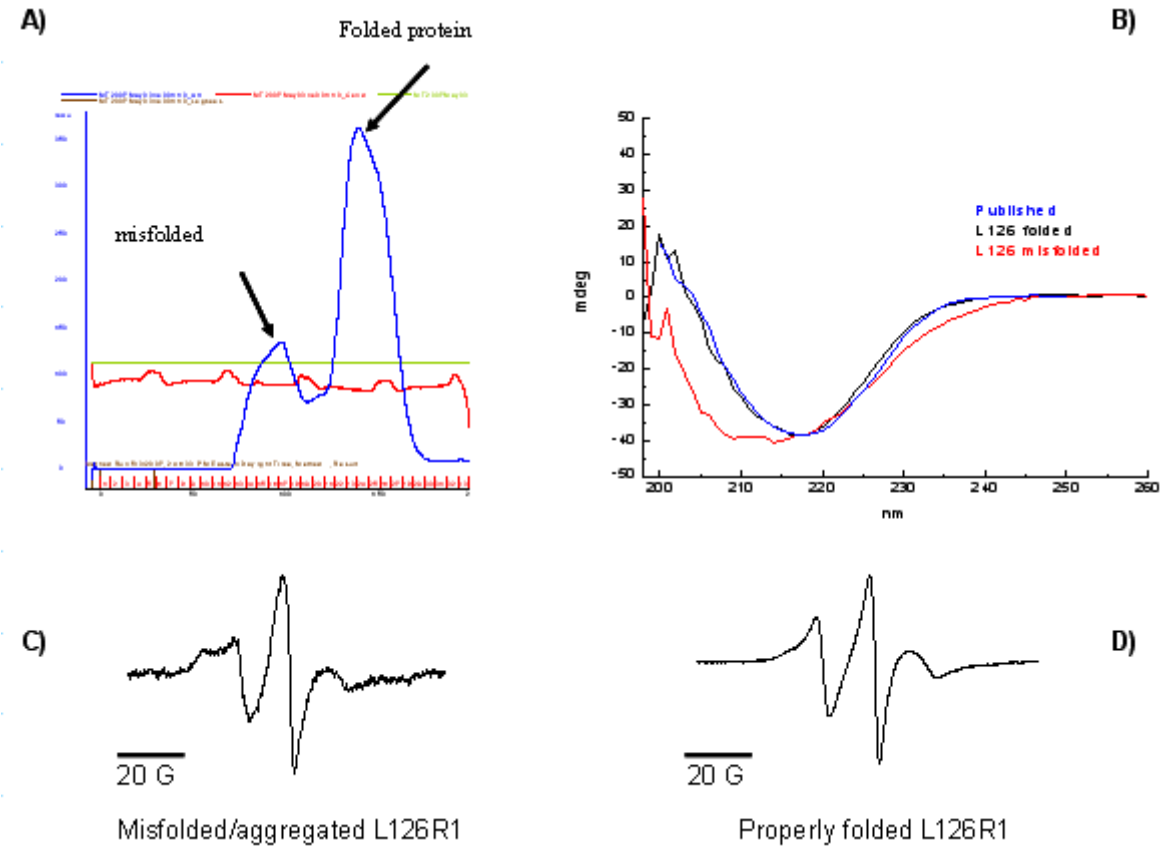

Figure 4-6. Gel filtration chromatogram showing separation of folded and misfolded GM2AP, circular dichroism (CD) spectra and EPR line shapes that show differences between folded and misfolded spin labeled GM2AP constructs.

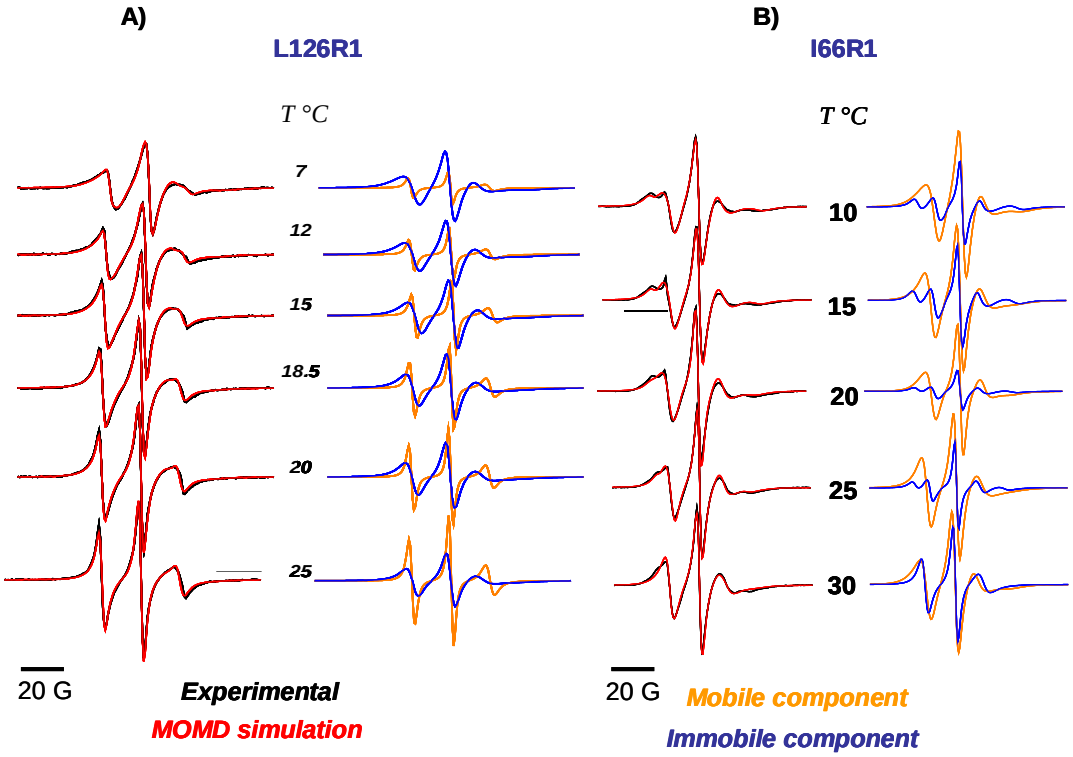

Figure 4-7. Overlay of the experimental and simulated solution EPR line shapes for L126R1 and I66R1 collected as a function of temperature, and the overlay of the mobile and immobile components for each spectrum.

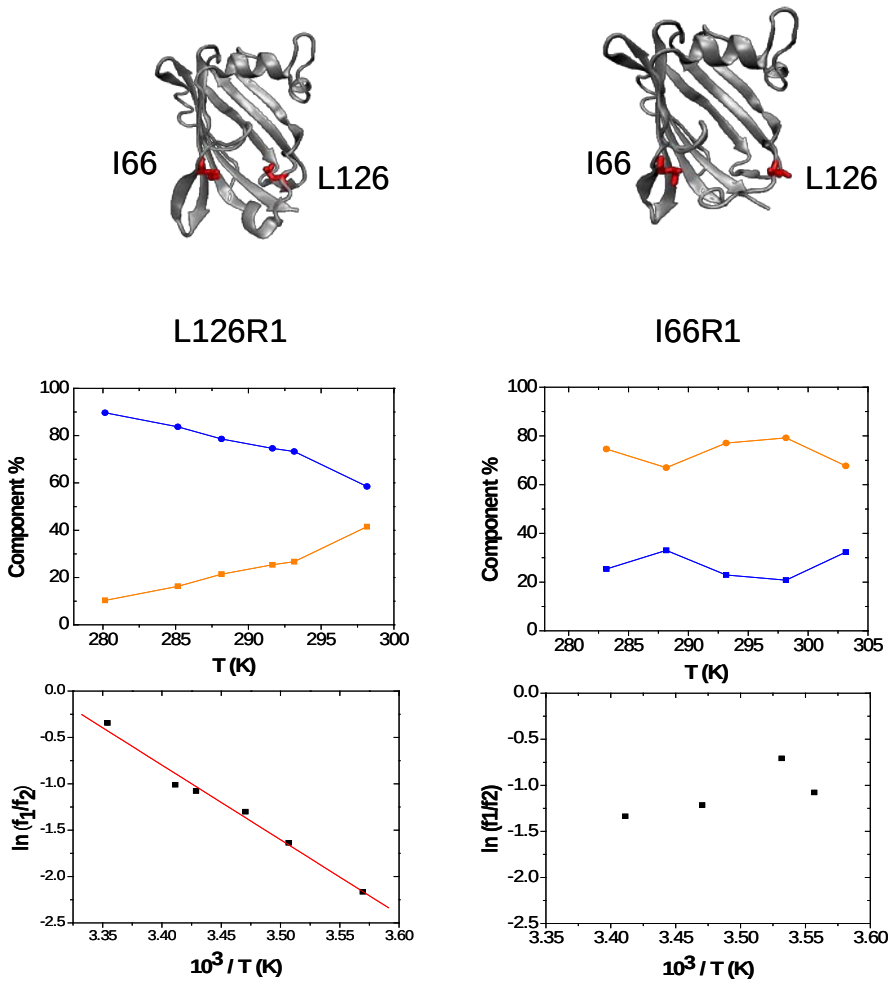

Figure 4-8. Plots of the percent mobile and immobile components obtained from MOMD simulations and plots showing temperature dependence of the fractions of the populations for L126R1 and I66R1.

CHAPTER 5
CONCLUSIONS AND FUTURE DIRECTION

Conclusions

The GM2 Activator Protein is an essential component of ganglioside catabolism. The protein functions at acidic pH, where it binds to GM2 in intralysosomal lipid vesicles and carries its ligand into solution as a protein:lipid complex for hydrolysis to GM3 by Hex A. Analysis of the crystal structure postulated that an apolar loop, spanning residues 59-61, could potentially penetrate into the lipid bilayer for lipid extraction. We have determined a membrane bound orientation of GM2AP on phosphatidylcholine bilayers by SDSL EPR and have shown that the orientation that occurs *in vitro* is different from that hypothesized from X-ray structure analysis. Rather than binding to vesicles in an upright fashion, GM2AP actually binds such that the entire face of the lipid binding pocket lies on the bilayer surface. This orientation is plausible since the role of GM2AP is to bind and solublize lipids and is consistent with other lipid binding proteins, like Sec14p.

We have also used site directed spin labeling to look at conformational changes of two flexible loop regions in GM2AP. The loop spanning residues 122 to 136, referred to as the "mobile loop," is seen in two different conformations in the X-ray structure that may reflect an "open" and "closed" state of the protein. Additionally, the "apolar loop" that spans residues 58 to 78 was identified from analysis of the X-ray structure as a flexible region of the protein. These two loops were of interest because they were identified as flexible regions of the protein and were hypothesized to be the sites that interacted with the lipids upon associating with the bilayer. We attached spin labels in these two loops to monitor a possible conformational change upon ligand binding. EPR spectra collected in the absence and presence of GM2 micelles showed no significant change in mobility of the spin label that correlated to a conformational change of

these loops upon ligand binding. The solution EPR line shapes were also simulated using a microscopic order macroscopic disorder (MOMD) model. The EPR spectra of spin labels attached in these two loops of GM2AP required two components for obtaining a best fit. Finally, variable temperature EPR experiments were performed using two of these sites (L126R1 on the mobile loop and I66 on the apolar loop) where EPR spectra for the two sites were collected at temperatures ranging from 5 ℃ to 35 ℃ and simulated. Spectral parameters obtained from the fittings were used to obtain thermodynamic information about the loops. We found that the apolar loop does not show a temperature dependant change in motion and the mobile loop appears to be in conformational exchange between the two positions seen in the X-ray structure. Gaining insight to the significance of the flexibility of the loops and to the orientation in which it binds to lipid bilayers in a pH dependant manner helps us to better understand how GM2AP binds and extracts lipids from bilayers.

Future Directions

Investigation of the Lipid Binding Cleft

Each of the spin labeled cysteine constructs in this work was tested for function by a fluorescence assay based upon the ability of the CYS variants to extract DDPHE from liposomes. We use the term “functional” assay, as opposed to “activity” assay because GM2AP is not an enzyme and, therefore, does not catalyze a reaction. The assay measures the rate of extraction of the fluorescently labeled lipid, DDHPE, by GM2AP, and the rates of DDHPE of extraction by spin labeled constructrs are compared to that of WT. A couple of the mutants (I66R1 and L128R1) were unable to extract DDHPE, even after reducing the spin label to ensure that the nitroxide was not simply quenching the fluorescence. We believe that attaching the nitroxide spin label in these locations sterically hinders the entrance to the hydrophobic binding pocket and thereby prevents GM2AP from binding DDHPE. A future direction for this project is

to investigate how the size of the amino acid side chains at the opening of the binding cavity affects the ability of GM2AP to extract DDHPE or other phospholipids. A systematic study would include site directed mutagenesis to individually mutate residues I66 and L128 to increasing sizes of hydrophobic side chains starting with the small side chain of alanine, followed by valine, then leucine (for I66) or isoleucine (for L128), and finally a large aromatic side chain phenylalanine. Phenylalanine was chosen over tryptophan to avoid potential quenching of the DDHPE fluorescence. Monitoring the ability of GM2AP to extract DDHPE as a function of side chain size could provide insight to the role of the native residues in lipid binding.

Power Saturation of GM2AP with Different Lipid Composition

In this work, we determined the membrane bound orientation of GM2AP on bilayers comprised of the neutral lipid POPC. It is known that in the late endosomes and lysosomes a relatively high concentration (15mol%) of the anionic lipid BMP is present. However, it is currently unknown the structures that form when BMP is mixed with phospholipid. But an anionic phospholipid like phosphatidylglycerol (PG) can be mixed with PC lipids to create negatively charged vesicles. In addition to charge, the membrane curvature is another variable that could affect GM2AP binding to bilayers. Lipids with small head groups such as phosphatidylethanolamine (PE) cause spontaneous negative curvature to bilayers. Analogous power saturation experiments to the ones presented in this work can be performed to study the effect of charge and membrane curvature on GM2AP binding to vesicles. We saw only surface association of GM2AP on PC bilayers, but perhaps the negatively charged vesicles causes the protein to associate closer to the membrane, or even penetrate into the lipid bilayer. Incorporating its specific ligand, GM2, would also be a very relevant set of experiments to perform.

Nuclear Magnetic Resonance Experiments

In this dissertation, a low resolution orientation of the GM2 activator protein on lipid bilayers is presented. A surface bound paramagnetic collider was required because GM2AP undergoes exchange on and off the bilayer surface. However, we currently do not know the rate at which GM2AP partitions on and off of the bilayer. Nuclear magnetic resonance (NMR) is another technique that may be more beneficial for determining the sites of GM2AP that interact with the vesicle surface in higher resolution. Our lab is now collecting heteronuclear single quantum coherence (HSQC) NMR spectra of ^{15}N labeled GM2AP in solution and determining the peak assignments for each amino acid. After the NMR assignments are made, HSQC NMR spectra can be collected for GM2AP mixed with GM2 micelles and with phosphatidylcholine liposomes. Amino acids that interact with the lipids can be identified by changes in the resonance peaks compared to the solution spectra.

APPENDIX A
VALUES OBTAINED FROM POWER SATURATION EXPERIMENTS

Table A-1. Raw data values obtained from power saturation experiments used to calculate collision parameters.

Mutant	$P_{1/2}$ Nitrogen	ΔHpp Nitrogen	$P_{1/2}$ Oxygen	ΔHpp Oxygen	$P_{1/2}$ NiEDDA	ΔHpp NiEDDA	$P_{1/2}$ DOGS-NTA-Ni pH 4.5	ΔHpp DOGS-NTA-Ni pH 4.5	$P_{1/2}$ DOGS-NTA-Ni + EDTA pH 4.5	ΔHpp DOGS-NTA-Ni + EDTA pH 4.5	$P_{1/2}$ DOGS-NTA-Ni pH 8.0	ΔHpp DOGS-NTA-Ni pH 8.0
V54R1	3.68	3.22	9.56	3.22	15.2	3.22	5.23	3.04	5.14	3.04	5.36	3.04
I66R1	3.47	2.44	9.49	2.50	18.36	2.50	4.64	2.60	4.97	2.60	5.13	2.60
T90R1	2.40	1.74	6.54	1.74	12.57	1.76	7.48	1.86	3.38	1.76	4.29	1.76
S115R1	2.83	3.03	8.22	2.44	10.51	2.54	4.26	3.13	3.99	3.13	4.09	3.13
L126R1	2.51	1.76	5.4	1.76	7.44	2.40	8.36	2.17	3.22	2.17	4.25	2.17
N136R1	2.36	2.05	6.8	2.05	13.49	2.05	6.57	2.05	4.59	2.05	3.98	2.05

APPENDIX B
PREPARATION OF NICKEL ETHYLEDIAMINEDIACETIC ACID

Nickel ethylenediaminediacetic acid (NiEDDA) for power saturation electron paramagnetic resonance (EPR) experiments was prepared according to (*52*). Briefly, equimolar amounts of nickel hydroxide ($Ni(OH)_2$) (464 mg) and ethylenediaminediacetic acid (EDDA) (881 mg) were mixed in 100 mL of methanol:water (50:50 v/v) and the solution was allowed to stir for 24 hours at room temperature in a covered beaker. After 24 hours, the temperature of the solution was increased to 60 °C and was allowed to stir for an additional 24 hours at 60 °C. The resulting NiEDDA solution was light blue and was not clear because some insoluble particles were still present. The solids were separated from the solution by centrifugation at about 18,000 *g* for 20 minutes. After centrifugation, the insoluble particles were in the "pellet" and the solution was blue and clear. The solvent was evaporated by rotovapping and submerging the vessel containing the sample in a warm water bath. The resulting crystals were collected and analyzed by elemental CHN analysis.

LIST OF REFERENCES

1. Gravel, R., Clarke, J., Kaback, M., Mahuran, D., Sandhoff, K., and Suzuki, K (1995) *The GM2 Gangliosidoses*, 7 ed., McGraw-Hill Inc., New York.

2. Sandhoff, K., and Kolter, T. (1996) *Trends Cell Biol 6*, 98-103.

3. Nagai, T. Y. a. Y. (1978) *Trends in Biochemical Sciences 3*, 128-131.

4. Thompson, L. K., Horowitz, P. M., Bentley, K. L., Thomas, D. D., Alderete, J. F., and Klebe, R. J. (1986) *J Biol Chem 261*, 5209-14.

5. Kielczynski, W., Harrison, L. C., and Leedman, P. J. (1991) *Proc Natl Acad Sci U S A 88*, 1991-5.

6. Kojima, N., and Hakomori, S. (1991) *J Biol Chem 266*, 17552-8.

7. Varki, N. M., and Varki, A. (2007) *Lab Invest 87*, 851-7.

8. Mahuran, D. J. (1998) *Biochim Biophys Acta 1393*, 1-18.

9. Ahn, V. E., Faull, K. F., Whitelegge, J. P., Fluharty, A. L., and Prive, G. G. (2003) *Proc Natl Acad Sci U S A 100*, 38-43.

10. Vaccaro, A. M., Salvioli, R., Tatti, M., and Ciaffoni, F. (1999) *Neurochem Res 24*, 307-14.

11. Rossmann, M., Schultz-Heienbrok, R., Behlke, J., Remmel, N., Alings, C., Sandhoff, K., Saenger, W., and Maier, T. (2008) *Structure 16*, 809-17.

12. Kolter, T., and Sandhoff, K. (2005) *Annu Rev Cell Dev Biol 21*, 81-103.

13. Morimoto, S., Martin, B. M., Yamamoto, Y., Kretz, K. A., O'Brien, J. S., and Kishimoto, Y. (1989) *Proc Natl Acad Sci U S A 86*, 3389-93.

14. Matsuda, J., Vanier, M. T., Saito, Y., Tohyama, J., and Suzuki, K. (2001) *Hum Mol Genet 10*, 1191-9.

15. Spiegel, R., Bach, G., Sury, V., Mengistu, G., Meidan, B., Shalev, S., Shneor, Y., Mandel, H., and Zeigler, M. (2005) *Mol Genet Metab 84*, 160-6.

16. Wilkening, G., Linke, T., Uhlhorn-Dierks, G., and Sandhoff, K. (2000) *J Biol Chem 275*, 35814-9.

17. Li, S. C., and Li, Y. T. (1976) *J Biol Chem 251*, 1159-63.

18. Vogel, A., Schwarzmann, G., and Sandhoff, K. (1991) *Eur J Biochem 200*, 591-7.

19. Kretz, K. A., Carson, G. S., Morimoto, S., Kishimoto, Y., Fluharty, A. L., and O'Brien, J. S. (1990) *Proc Natl Acad Sci U S A 87*, 2541-4.

20. de Alba, E., Weiler, S., and Tjandra, N. (2003) *Biochemistry 42*, 14729-40.

21. Sano, A., and Radin, N. S. (1988) *Biochem Biophys Res Commun 154*, 1197-203.

22. Vaccaro, A. M., Tatti, M., Ciaffoni, F., Salvioli, R., Barca, A., and Scerch, C. (1997) *J Biol Chem 272*, 16862-7.

23. Klein, A., Henseler, M., Klein, C., Suzuki, K., Harzer, K., and Sandhoff, K. (1994) *Biochem Biophys Res Commun 200*, 1440-8.

24. Linke, T., Wilkening, G., Sadeghlar, F., Mozcall, H., Bernardo, K., Schuchman, E., and Sandhoff, K. (2001) *J Biol Chem 276*, 5760-8.

25. Morimoto, S., Martin, B. M., Kishimoto, Y., and O'Brien, J. S. (1988) *Biochem Biophys Res Commun 156*, 403-10.

26. Popovic, K., and Prive, G. G. (2008) *Acta Crystallogr D Biol Crystallogr 64*, 589-94.

27. Bruhn, H. (2005) *Biochem J 389*, 249-57.

28. Chang, R., Nir, S., and Poulain, F. R. (1998) *Biochim Biophys Acta 1371*, 254-64.

29. Poulain, F. R., Allen, L., Williams, M. C., Hamilton, R. L., and Hawgood, S. (1992) *Am J Physiol 262*, L730-9.

30. Wendeler, M., Hoernschemeyer, J., John, M., Werth, N., Schoeniger, M., Lemm, T., Hartmann, R., Kessler, H., and Sandhoff, K. (2004) *Protein Expr Purif 34*, 147-57.

31. Wright, C. S., Li, S. C., and Rastinejad, F. (2000) *J Mol Biol 304*, 411-22.

32. Wendeler, M., Werth, N., Maier, T., Schwarzmann, G., Kolter, T., Schoeniger, M., Hoffmann, D., Lemm, T., Saenger, W., and Sandhoff, K. (2006) *FEBS J 273*, 982-91.

33. Wright, C. S., Mi, L. Z., and Rastinejad, F. (2004) *J Mol Biol 342*, 585-92.

34. Conzelmann, E., and Sandhoff, K. (1979) *Hoppe Seylers Z Physiol Chem 360*, 1837-49.

35. Conzelmann, E., Burg, J., Stephan, G., and Sandhoff, K. (1982) *Eur J Biochem 123*, 455-64.

36. Ran, Y., and Fanucci, G. E. (2008) *Anal Biochem 382*, 132-4.

37. Kytzia, H. J., and Sandhoff, K. (1985) *J Biol Chem 260*, 7568-72.

38. Novak, A., Lowden, J. A., Gravel, Y. L., and Wolfe, L. S. (1979) *J Lipid Res 20*, 678-81.

39. Smiljanic-Georgijev, N., Rigat, B., Xie, B., Wang, W., and Mahuran, D. J. (1997) *Biochim Biophys Acta 1339*, 192-202.

40. Werth, N., Schuette, C. G., Wilkening, G., Lemm, T., and Sandhoff, K. (2001) *J Biol Chem 276*, 12685-90.

41. Kuwana, T., Mullock, B. M., and Luzio, J. P. (1995) *Biochem J 308 (Pt 3)*, 937-46.

42. Rigat, B., Reynaud, D., Smiljanic-Georgijev, N., and Mahuran, D. (1999) *Biochem Biophys Res Commun 258*, 256-9.

43. Lemieux, M. J., Mark, B. L., Cherney, M. M., Withers, S. G., Mahuran, D. J., and James, M. N. (2006) *J Mol Biol 359*, 913-29.

44. Yadao, F., Hechtman, P., and Kaplan, F. (1997) *Biochim Biophys Acta 1340*, 45-52.

45. Sandhoff, K., Andreae, U., and Jatzkewitz, H. (1968) *Life Sci 7*, 283-8.

46. Schroder, M., Schnabel, D., Suzuki, K., and Sandhoff, K. (1991) *FEBS Lett 290*, 1-3.

47. Xie, B., Rigat, B., Smiljanic-Georgijev, N., Deng, H., and Mahuran, D. (1998) *Biochemistry 37*, 814-21.

48. Fanucci, G. E., and Cafiso, D. S. (2006) *Curr Opin Struct Biol 16*, 644-53.

49. McHaourab, H. S., Lietzow, M. A., Hideg, K., and Hubbell, W. L. (1996) *Biochemistry 35*, 7692-704.

50. Weil, J. A., Bolton, James R., Wertz, John E. (1994) *Electron Paramagnetic Resonance: Elementary Theory and Practical Applications*, John Wiley & Sons, Inc., New York.

51. Morin, B., Bourhis, J. M., Belle, V., Woudstra, M., Carriere, F., Guigliarelli, B., Fournel, A., and Longhi, S. (2006) *J Phys Chem B 110*, 20596-608.

52. Altenbach, C., Greenhalgh, D. A., Khorana, H. G., and Hubbell, W. L. (1994) *Proc Natl Acad Sci U S A 91*, 1667-71.

53. Frazier, A. A., Roller, C. R., Havelka, J. J., Hinderliter, A., and Cafiso, D. S. (2003) *Biochemistry 42*, 96-105.

54. Macosko, J. C., Kim, C. H., and Shin, Y. K. (1997) *J Mol Biol 267*, 1139-48.

55. Oh, K. J., Zhan, H., Cui, C., Altenbach, C., Hubbell, W. L., and Collier, R. J. (1999) *Biochemistry 38*, 10336-43.

56. Fanucci, G. E., Cadieux, N., Piedmont, C. A., Kadner, R. J., and Cafiso, D. S. (2002) *Biochemistry 41*, 11543-51.

57. Koteiche, H. A., Reeves, M. D., and McHaourab, H. S. (2003) *Biochemistry 42*, 6099-105.

58. Chiang, Y. W., Borbat, P. P., and Freed, J. H. (2005) *J Magn Reson 172*, 279-95.

59. Galiano, L., Bonora, M., and Fanucci, G. E. (2007) *J Am Chem Soc 129*, 11004-5.

60. Altenbach, C., Froncisz, W., Hemker, R., McHaourab, H., and Hubbell, W. L. (2005) *Biophys J 89*, 2103-12.

61. Frazier, A. A., Wisner, M. A., Malmberg, N. J., Victor, K. G., Fanucci, G. E., Nalefski, E. A., Falke, J. J., and Cafiso, D. S. (2002) *Biochemistry 41*, 6282-92.

62. Zhao, M., Zen, K. C., Hernandez-Borrell, J., Altenbach, C., Hubbell, W. L., and Kaback, H. R. (1999) *Biochemistry 38*, 15970-7.

63. Furst, W., and Sandhoff, K. (1992) *Biochim Biophys Acta 1126*, 1-16.

64. Ran, Y. a. F., G. E. (submitted) *Biophys J*.

65. Giehl, A., Lemm, T., Bartelsen, O., Sandhoff, K., and Blume, A. (1999) *Eur J Biochem 261*, 650-8.

66. Gross, A., and Hubbell, W. L. (2002) *Biochemistry 41*, 1123-8.

67. Herrick, D. Z., Sterbling, S., Rasch, K. A., Hinderliter, A., and Cafiso, D. S. (2006) *Biochemistry 45*, 9668-74.

68. Perozo, E., Cortes, D. M., Sompornpisut, P., Kloda, A., and Martinac, B. (2002) *Nature 418*, 942-8.

69. Kirby, T. L., Karim, C. B., and Thomas, D. D. (2004) *Biochemistry 43*, 5842-52.

70. Dong, J., Yang, G., and McHaourab, H. S. (2005) *Science 308*, 1023-8.

71. Perozo, E., Cortes, D. M., and Cuello, L. G. (1998) *Nat Struct Biol 5*, 459-69.

72. Canaan, S., Nielsen, R., Ghomashchi, F., Robinson, B. H., and Gelb, M. H. (2002) *J Biol Chem 277*, 30984-90.

73. Smirnova, T. I., Chadwick, T. G., MacArthur, R., Poluektov, O., Song, L., Ryan, M. M., Schaaf, G., and Bankaitis, V. A. (2006) *J Biol Chem 281*, 34897-908.

74. Smirnova, T. I., Chadwick, T. G., Voinov, M. A., Poluektov, O., van Tol, J., Ozarowski, A., Schaaf, G., Ryan, M. M., and Bankaitis, V. A. (2007) *Biophys J 92*, 3686-95.

75. Ladokhin, A. S., Jayasinghe, S., and White, S. H. (2000) *Anal Biochem 285*, 235-45.

76. Svennerholm, L. (1957) *Biochim Biophys Acta 24*, 604-11.

77. Wright, C. S., Zhao, Q., and Rastinejad, F. (2003) *J Mol Biol 331*, 951-64.

78. Hubbell, W. L. a. A., C. (1994) *Curr Opin Struct Biol 4*, 566-573.

79. Zhou, D., Cantu, C., 3rd, Sagiv, Y., Schrantz, N., Kulkarni, A. B., Qi, X., Mahuran, D. J., Morales, C. R., Grabowski, G. A., Benlagha, K., Savage, P., Bendelac, A., and Teyton, L. (2004) *Science 303*, 523-7.

80. Hubbell, W. L., Cafiso, D. S., and Altenbach, C. (2000) *Nat Struct Biol 7*, 735-9.

81. Fanucci, G. E., Coggshall, K. A., Cadieux, N., Kim, M., Kadner, R. J., and Cafiso, D. S. (2003) *Biochemistry 42*, 1391-400.

82. Budil, D. E., Lee, S., Saxena, S., Freed, J. H. (1996) *J Magn Reson 120*, 155-189.

83. Columbus, L., and Hubbell, W. L. (2004) *Biochemistry 43*, 7273-87.

84. Bordignon, E., Klare, J. P., Doebber, M., Wegener, A. A., Martell, S., Engelhard, M., and Steinhoff, H. J. (2005) *J Biol Chem 280*, 38767-75.

BIOGRAPHICAL SKETCH

Jordan Delyn Mathias was born in Portsmouth, VA. As a child, she took piano and ballet lessons and played on a soccer team. After one summer camp that offered both soccer and horseback riding, Jordan began taking horseback riding lessons and participating in local horse shows. She was involved in the 4H Horse and Pony Club, through which she took her first horse, Lilley, to the District and State Fair Horse Shows. In addition to her involvement with horses and 4H, Jordan also played the viola in the Western Branch Middle School and High School Orchestras.

Jordan attended Mary Washington College for her undergraduate studies. She rode for the MWC Equestrian Team for two years and, in her second year on the team, qualified to compete in the Zones competition after winning her division that season. She participated in the Summer Research Program at MWC following her junior year in college where she studied DNA topology by agarose gel electrophoresis and by atomic force microscopy. Jordan graduated with her Bachelor of Science degree in chemistry from Mary Washington College in May 2003.

After working in industry for one year as a technical writer, Jordan continued her education at the University of Florida and earned her Ph.D. in Chemistry under the direction of Gail E. Fanucci, Ph.D. Through her graduate studies, she has been able to present her research at local, regional and national meetings, be involved in writing manuscripts, as well as explore her enthusiasm for teaching through instructing undergraduate labs as well as a full lecture. Jordan is pursuing an academic career as an Assistant Professor at Marietta College in Marietta, OH.